J. Fluid Mech. (2010), *vol.* 642, *pp.* 49–77.
doi:10.1017/S0022112009991674

Turbulent plumes with heterogeneous chemical reaction on the surface of small buoyant droplets

SILVANA S. S. CARDOSO† AND SEAN T. MCHUGH

Department of Chemical Engineering and Biotechnology, University of Cambridge, Pembroke Street, Cambridge CB2 3RA, UK

(Received 30 November 2008; revised 13 August 2009; accepted 14 August 2009; first published online 30 November 2009)

A model is developed for a turbulent plume with heterogeneous chemical reaction rising in an unbounded environment. The chemical reaction, which may generate or deplete buoyancy in the plume, occurs at the interface between two phases, a continuous phase and a dispersed one. We study the case in which a buoyant reactant is released at the source and forms the dispersed phase, consisting of very small bubbles, droplets or particles. Once in contact with the ambient fluid, a first-order irreversible reaction takes place at the surface of the, for example, droplets. The behaviour of this plume in a uniform and stratified environment is examined. We show that the dynamics of a pure plume with such heterogeneous reaction is completely determined by the ratio of the environmental buoyancy frequency N and a frequency parameter associated with the chemical reaction, G. The group G is a measure of the ability of the reaction to generate buoyancy in the plume. In a uniform environment, the sign of parameter G fully determines the plume motion. When the reaction generates buoyancy (positive G) the motion is unbounded, whilst when reaction depletes buoyancy (negative G) the plume reaches a level of neutral buoyancy. A relation for this neutral buoyancy level as a function of the initial buoyancy flux of the plume and G is calculated. Our theoretical predictions compared well with experimental results using a plume of calcium carbonate particles descending in an acidic aqueous solution. In a stratified environment, the motion of the plume is always bounded, irrespective of the magnitude of G, and we determine the level of maximum buoyancy flux, as well as those of zero buoyancy and zero momentum as a function of N/G. Finally, our model is applied to study the dynamics of a localized release of carbon dioxide in the ocean.

Key words: plumes/thermals, turbulent reacting flows

1. Introduction

Density differences play an important role in many geophysical and industrial flows. If the source of buoyancy is localized, the motion may develop in the form of a plume. Examples of turbulent plumes linked to industrial activity include discharges of smoke from chimneys, effluents from submerged pollutant outlets and leaks from pipelines transporting chemicals. In geophysics, plumes are encountered above seafloor hydrothermal vents, in convective clouds and in explosive volcanic eruptions. These flows range over orders of magnitude in scale, but their dynamics are similar.

† Email address for correspondence: sssc1@cam.ac.uk

As a turbulent plume rises, it entrains ambient fluid and expands radially. In an environment of uniform density the buoyancy flux in the plume is constant and the flow is unbounded. However, in a stratified environment where density decreases with height, the buoyancy flux in the plume decreases with ascent distance. As a result, the plume comes to rest at a finite height and spreads out radially. The effects of ambient stratification on the dynamics of a plume and on its maximum height of rise have been studied extensively in the past (Morton, Taylor & Turner 1956; Turner 1979). However, in addition to external density stratification, many processes occurring inside natural and industrial plumes may lead to the generation or depletion of buoyancy. For example, in fires and other chemical plumes, the ongoing chemical reactions generate large fluxes of heat within the plume; in volcanic plumes, hot clasts heat up entrained air generating the buoyancy responsible for the large heights of rise in the atmosphere; in clouds and in evaporative cooling processes, transitions of phase can induce important density changes. These types of plumes, with internally produced buoyancy changes, have been the focus of comparatively few studies.

In the laboratory, water and a mixture of methanol and ethylene glycol (MEG), or a mixture of ethanol and ethylene glycol (EEG), has been used to create a fluid whose density changes non-monotonically with composition. Turner (1966), Woods & Caulfield (1992) and, more recently, Kaminski, Tait & Carazzo (2005) explored the non-ideality of these liquid mixtures to study plumes and jets with reversing buoyancy. The first two studies were concerned with identifying the conditions for which the flow collapses, while the last one focused on the effect of the Richardson number on entrainment into a jet. In the gas phase, Bhat & Narasimha (1996) and Agrawal & Prasad (2004) conducted experiments on volumetrically heated jets, using electrical wires over a limited vertical extent of the flow. Their results showed that a rapid buoyancy increase caused by thermal expansion led to a decrease in the rate of radial spreading of the jet. This effect was associated with an acceleration of the gas and a disruption of the eddy structure.

On the theoretical side, a few studies have considered plumes with internal generation of buoyancy. Hunt & Kaye (2005) examined the behaviour of lazy plumes with an internal buoyancy flux gain. They considered a source of buoyancy flux which increased linearly with height. Their results showed that a plume with such internal generation of buoyancy is narrower than a pure plume and has constant velocity, independent of height, in the far field. Ishimine (2007) extended this work and examined a plume with a bounded increase in buoyancy flux as a function of height. He noted that, close to the source, the plume behaved as one with a linear increase in buoyancy flux, whilst it approached asymptotically the behaviour of a pure plume farther downstream. Whilst the studies above relied on the entrainment assumption of Morton *et al.* (1956) or assumed the plume radius to be directly proportional to height (Ishimine 2007; Batchelor 1954), a different integral method was presented by Diez & Dahm (2007) to determine the effects of buoyancy generation on flame behaviour. They developed an equation for the centreline velocity in inert and reactive jets and plumes in terms of the local flow width, thus avoiding the use of the entrainment coefficient. They then showed through scaling that the flow width is proportional to height in the case of both inert and reactive plumes. They also provided power-law scalings for the momentum-dominated and buoyancy-dominated limits. Comparison of their theoretical predictions with buoyant flame data showed excellent agreement. Conroy & Llewellyn Smith (2008) have very recently proposed a model for chemically reacting plumes. They examined a second-order non-reversible reaction between the source plume chemical and another species in the ambient. The internal change of buoyancy in the plume arises due to both thermal and chemical composition changes

occurring during reaction. In this case, the source term for buoyancy is proportional to the local fluxes of the two reactants and inversely proportional to the flux of momentum. Their results show that for an exothermic reaction the plume is lazy, whereas for an endothermic reaction it behaves jet-like.

There have also been a few studies on the effects of a time-dependent buoyancy flux at the source on the behaviour of plumes and jets, in both uniform and stratified environments. For pure plumes and jets, Scase, Caulfield & Dalziel (2006*a*) and Scase *et al.* (2006*b*) found a class of separable solutions and showed that when the source strength is reduced, a region of narrowing radius develops in the flow. More recently, this theory was generalized in Scase, Caulfield & Dalziel (2008) to consider the temporal behaviour of plumes emerging from a finite source which undergoes a sudden reduction in buoyancy flux. Their model was complemented by experimental results, showing that the plume never totally pinches off into thermals.

The studies described above have considered buoyancy generation/depletion either in a source term of specified form in the buoyancy equation, in the boundary conditions, or arising from a homogeneous chemical reaction in a single-phase plume. However, in volcanic eruptions, in clouds, in evaporative cooling processes and in many chemical plumes, buoyancy may be generated through the interaction of two phases – a continuous one and a dispersed one. The interface between the two phases plays an important role in such cases. The internal source of buoyancy is in these cases heterogeneous (i.e. more than one phase is involved) and has a different dynamics to the homogeneous sources considered hitherto.

The principal motivation for the present study has been to understand the dynamics of a carbon dioxide release in the ocean. Such a release could occur following an accidental leakage of CO_2 from a geological storage site under the sea bed. A localized continuous release would form a rising plume of CO_2 droplets or bubbles, depending on the release depth. Plumes of CO_2 droplets in the deep ocean have several characteristics that set them apart from the previously studied two-phase plumes. The CO_2 bubbles/droplets dissolve in seawater, increasing the density of the plume liquid. In addition, at higher pressures, reaction with seawater can form CO_2 hydrates, an exothermic process. The dynamics and eventual fate of the CO_2 plume depend critically on the rate of internal buoyancy changes caused by such dissolution and reaction between the CO_2 and the seawater.

The aim of this work is therefore to study theoretically a plume that is influenced by buoyancy generation resulting from chemical reaction between different phases, dissolution or phase-transition. The dynamics of such a plume in an environment with uniform density, as well in a linear density stratification, is considered theoretically. Particle image velocimetry (PIV) measurements of a particle-laden plume with chemical reaction, in a uniform environment, are also presented and compared with the theory. Finally, our results are applied to examine the behaviour of a release of carbon dioxide in the ocean.

2. Theory

2.1. *Chemical reaction and density change*

Consider a plume of very small buoyant droplets of chemical species A rising in a stagnant liquid environment of species X. Chemical A is immiscible with X. As a droplet rises, the chemical reaction

$$|\nu_A|A + X \rightarrow |\nu_B|B \tag{2.1}$$

takes place at its surface. Here, ν_A and ν_B are stoichiometric coefficients defined as being positive for products and negative for reactants. We assume that chemical X is in great excess to the stoichiometric requirements of the reaction. Product B may either dissolve in X or form a separate phase, such as small bubbles or crystals. The external environment may be stratified in density owing to the presence of an inert chemical S, which is soluble in X.

We shall need to quantify the concentration of reactant A at two levels, *viz*. the droplet level and the plume level. Given that inside each droplet A is pure, the concentration of A in the droplet in mass per unit volume is equal to the density of A, ρ_A; this concentration is important in determining the reaction rate. Thus the rate of reaction per unit surface area of droplet, with respect to species A, is given by

$$r_A = \nu_A k \rho_A, \tag{2.2}$$

where k is the kinetic constant. In SI units, r_A is measured in kg m^{-2} s^{-1}, k in ms^{-1} and ρ_A in kg m^{-3}. At the plume level, the average concentration of A is calculated over a sufficiently large volume to contain many droplets, but much smaller than the plume's scale. This concentration will be denoted by c_A and is important in the calculation of the local average density of the plume mixture. In general, the concentration of species i in mass per unit volume of the plume mixture is denoted by c_i.

The density of a small volume of plume mixture can change with time owing to compositional and thermal changes of the mixture, associated with mixing and/or reaction. Following the motion of a small volume of the plume mixture, its density varies according to

$$\frac{\mathrm{D}\rho}{\mathrm{D}t} = \rho \sum_{i=1}^{4} \left[\frac{\beta}{C_p} \left(\frac{\partial h}{\partial c_i} \right)_{p,T,j\neq i} - \rho \left(\frac{\partial \rho^{-1}}{\partial c_i} \right)_{p,T,j\neq i} \right] \frac{\mathrm{D}c_i}{\mathrm{D}t}. \tag{2.3}$$

Here, h is the specific enthalpy, β is the thermal expansion coefficient and C_p the specific heat, of the mixture. The summation has been taken over the four species A, X, B and S described above. Equation (2.3) was derived in Clarke & McChesney (1964) and was recently used straightforwardly by Conroy & Llewellyn Smith (2008) in the context of a perfect gas plume with homogeneous chemical reaction. However, it is important to note here that the first term in the square brackets accounts for two effects: (i) the enthalpy changes associated with the mixing of the components (a change of intermolecular forces); and (ii) the enthalpy changes arising from chemical reaction (a change of bonds in the molecules). Mixing effects are important in non-ideal mixtures, such as the MEG and EEG mixtures used in the experiments by Turner (1966) and Woods & Caulfield (1992), previously mentioned in the introduction; in these mixtures the intermolecular forces change significantly with a change in concentration, resulting in, for example, a nonlinear variation of the density of the mixture with composition. However, for dilute systems, in which the solvent is present in great excess relative to the other chemicals, the density changes associated with mixing are small (see e.g. Sandler 1999). In this case, only the effects of reaction on enthalpy need to be taken into account. Then we can write

$$\Delta H_r = \rho \sum_{i=1}^{2} \left[\left(\frac{\partial h}{\partial c_i} \right)_{p,T,j\neq i} \frac{\mathrm{d}c_i}{\mathrm{d}c_A} \right], \tag{2.4}$$

where ΔH_r is the heat of reaction per unit volume of mixture and per amount of A consumed, and is taken as positive for an endothermic reaction. Using (2.4) and

noting that $\mathrm{d}c_B/\mathrm{d}c_A = \nu_B M_B/(\nu_A M_A)$ from the stoichiometry of the reaction, (2.3) simplifies to

$$\frac{\mathrm{D}\rho}{\mathrm{D}t} = \left[\frac{\beta(\Delta H_r)}{C_p} + \sum_{i=1}^{2} K_i \frac{\nu_i M_i}{\nu_A M_A}\right] \frac{\mathrm{D}c_A}{\mathrm{D}t}, \tag{2.5}$$

where

$$K_i = -\rho^2 \left(\frac{\partial \rho^{-1}}{\partial c_i}\right)_{p,T,j\neq i}. \tag{2.6}$$

For chemical species in a different phase from the solvent, the coefficients K_i are readily calculated from (2.6). For dissolved species, these coefficients need to be determined experimentally in general. The summation in (2.4) and (2.5) has now been taken over only the two species whose concentrations change during reaction, namely A and B.

We need further to express $\mathrm{D}c_A/\mathrm{D}t$ in (2.5) in terms of the surface reaction rate in (2.2). For spherical droplets of radius R,

$$\frac{\mathrm{D}c_A}{\mathrm{D}t} = r_A \frac{S_a}{V} = r_A \frac{4\pi R^2}{V} \frac{m_A}{4/3\pi R^3 \rho_A} = r_A \frac{3c_\mathrm{A}}{R\rho_\mathrm{A}}, \tag{2.7}$$

where S_a is the surface area available for reaction, V is the volume of the mixture and m_A is the mass of A. Substituting (2.7) into (2.5), the rate of change of density of the mixture as a result of heterogeneous chemical reaction occurring on the surface of spherical drops is obtained:

$$\frac{\mathrm{D}\rho}{\mathrm{D}t} = \left[\frac{\beta(\Delta H_r)}{C_p} + \sum_{i=1}^{2} K_i \frac{\nu_i M_i}{\nu_A M_A}\right] r_A \frac{3c_\mathrm{A}}{R\rho_\mathrm{A}}. \tag{2.8}$$

2.2. *Plume conservation equations*

We assume the plume of small droplets issues from a localized, horizontal source of A and is axisymmetrical. The flow in the plume is composed of two phases, the dispersed buoyant droplets and a continuous phase consisting mainly of ambient liquid. The droplets typically rise faster than the continuous phase, by a slip velocity u_s. It has been shown experimentally that the structure of such a two-phase plume depends critically on the relative magnitude of u_s and the convective velocity in the plume W. When $u_s/W \geqslant 1$, the droplets form an inner circular plume surrounded by an annular outer plume containing only the continuous phase. The buoyancy is concentrated within the central region and momentum is imparted to the surrounding liquid via turbulent shear stresses (McDougall 1978; Asaeda & Imberger 1993). When $u_s/W \ll 1$, the dispersed phase is carried passively and remains widely distributed in the plume flow (Chen & Cardoso 2000; Socolofsky & Adams 2005). The integral theory for two-phase plumes (see Milgram 1983) is similar to the classical theory for single-phase plumes of Morton *et al.* (1956). The governing equations express conservation of volume, momentum and buoyancy for the two phases, and the radial distributions of velocity and buoyancy are assumed to be Gaussian. Four parameters are usually required: the droplet slip velocity u_s, the ratio of the widths of the velocity and buoyancy profiles λ, the entrainment coefficient α and the ratio of the total momentum flux to the momentum flux carried by the mean flow, which is called the momentum amplification factor γ. While in single-phase plumes typically $\gamma \sim 1.1$ (Chen & Rodi 1980), for bubble plumes the momentum amplification factor has been shown to increase with bubble diameter and values as high as 2.8 have been measured

(Milgram 1983). The parameter γ accounts therefore for the effect of the interaction of the phases on the turbulent momentum transport in the plume.

In this study, we extend the modelling approach of Morton *et al.* (1956) to a two-phase plume with buoyancy generation owing to chemical reaction at the interface between the phases. We shall consider the contribution from the turbulent fluxes of momentum, energy and chemical species in the plume, but assume that u_s/W is sufficiently small for the dispersed phase to remain well distributed radially, so that $\lambda \approx 1$. The motion of such a two-phase plume in both uniform and stratified environments is analysed below. We should note that in a stratified environment, the flow is further complicated by phase-separation above the neutral buoyancy level. Indeed, in this region the plume velocity becomes smaller than the slip velocity of the droplets, allowing the droplets to separate and form a new plume (Asaeda & Imberger 1993; Socolovsky & Adams 2005). The plume fluid then spreads radially forming a lateral intrusion. The models described above, as well as the model developed in this study, are therefore valid only up to the level of neutral buoyancy, or more generally, a level where phase separation occurs.

The time-averaged conservation equations for steady flow of the two-phase mixture may be written as

$$\frac{1}{r}\frac{\partial (ru)}{\partial r} + \frac{\partial w}{\partial z} = 0, \tag{2.9a}$$

$$\gamma \rho_r \left(u\frac{\partial w}{\partial r} + w\frac{\partial w}{\partial z} \right) = -\frac{\partial p}{\partial z} - \rho g, \tag{2.9b}$$

$$\gamma \left(u\frac{\partial \rho}{\partial r} + w\frac{\partial \rho}{\partial z} \right) = \left[\frac{\beta (\Delta H_r)}{C_p} + \sum_{i=1}^{2} K_i \frac{\nu_i M_i}{\nu_A M_A} \right] r_A \frac{3c_{\mathrm{A}}}{R\rho_{\mathrm{A}}}, \tag{2.9c}$$

$$\gamma \left(u\frac{\partial c_i}{\partial r} + w\frac{\partial c_i}{\partial z} \right) = \nu_i k c_i \frac{3}{R}\frac{M_i}{M_A} \tag{2.9d}$$

for volume, vertical momentum, energy and chemical species, respectively. Here u and w are the time-averaged radial and vertical velocities, and r and z are the radial and vertical coordinates. The time-averaged pressure, density of the plume mixture and concentration of species i are p, ρ and c_i, respectively; g is the acceleration of gravity. The reference density ρ_r is taken to be the density of the environment ρ_e at the level of the source. The formulation of these equations assumes the Boussinesq approximation holds. The turbulent transport factor γ expresses the ratio of the total fluxes of momentum, energy and chemical species to the corresponding mean fluxes. Milgram (1983) studied inert, two-phase plumes in a uniform environment and therefore measured the turbulent transport of momentum only. In the absence of further measurements for the turbulent transport of energy and chemical species in multiphase plumes, we shall assume here that γ is the same for all three fluxes based on experimental results for single-phase plumes and jets (Chen & Rodi 1980; Wang & Law 2002). For $\gamma = 1$, (2.9*a*,*b*) reduce to the situation analysed by Morton *et al.*, (1956). The right-hand sides of (2.9*c*,*d*) account for the effects of reaction; they differ from the equations recently derived by Conroy & Llewellyn Smith (2008) because the reaction here occurs at an interface and not in the bulk continuous phase.

The plume behaviour can be described in terms of the mean fluxes of volume Q, momentum M, buoyancy B and mass of reactant A, F_A. Assuming Gaussian profiles

of equal widths for velocity and concentration in the plume, these fluxes are given by

$$Q(z) = \int_0^\infty 2\pi r w \, \mathrm{d}r = \pi b^2 w_c, \tag{2.10a}$$

$$M(z) = \int_0^\infty 2\pi r w^2 \, \mathrm{d}r = \frac{1}{2}\pi b^2 w_c^2, \tag{2.10b}$$

$$B(z) = \int_0^\infty 2\pi r w g' \, \mathrm{d}r, \tag{2.10c}$$

$$F_A(z) = \int_0^\infty 2\pi r w c_A \, \mathrm{d}r = \frac{1}{2}\pi b^2 w_c c_{Ac}. \tag{2.10d}$$

Here b is the radius of the plume and $g' = g(\rho_e - \rho)/\rho_r$ is the reduced gravity. The subscript c denotes the time-averaged property at the centreline of the plume. If the plume and the environment are initially free from species B, the flux of B is related to the flux of A via the stoichiometry of the reaction, $F_B = -(F_{A0} - F_A)\nu_B/\nu_A$; the subscript 0 refers to the flux at the source of the plume ($z = 0$). The fluxes of inert species S and solvent X in the plume could be obtained in the same way as that of A, but we shall see that these are unimportant in the present work. The assumption of Gaussian profiles above is valid provided the time scale for reaction is larger than the Kolmogorov time scale for the turbulent mixing by the small-scale eddies in the plume. This can be expressed as $R/k \gg (\nu/\varepsilon)^{1/2}$ or $Da = (\nu/\varepsilon)^{1/2}k/R \ll 1$, where Da is the Damkohler number, ν is the viscosity of the plume mixture and ε is the turbulent energy dissipation.

Using (2.9) and (2.10), the variation of the mean fluxes of volume, momentum, buoyancy and species A, with height in the plume, are given by

$$\frac{\mathrm{d}Q}{\mathrm{d}z} = (8\pi\alpha^2)^{1/2} M^{1/2}, \tag{2.11}$$

$$\frac{\mathrm{d}M}{\mathrm{d}z} = \frac{1}{\gamma}\frac{BQ}{M}, \tag{2.12}$$

$$\frac{\mathrm{d}B}{\mathrm{d}z} = -N^2 Q + \frac{1}{\gamma} G B_0 \frac{Q}{M}\frac{F_A}{F_{A0}}, \tag{2.13}$$

$$\frac{\mathrm{d}F_A}{\mathrm{d}z} = \frac{3k\nu_A}{R}\frac{1}{\gamma}\frac{Q}{M}F_A, \tag{2.14}$$

where the entrainment coefficient α (for Gaussian profiles) is taken to be constant,

$$N = \left(-\frac{g}{\rho_r}\frac{\mathrm{d}\rho_e}{\mathrm{d}z}\right)^{1/2}$$

is the buoyancy frequency in the environment and

$$G = -\frac{3k\nu_A}{R}\frac{\rho_A}{\rho_r - \rho_A}\left(\frac{\beta(\Delta H_r)}{C_p} + \sum_{i=1}^{2} K_i \frac{\nu_i M_i}{\nu_A M_A}\right). \tag{2.15}$$

In the derivation of (2.13), it has been assumed that the coefficients K_i (cf. (2.6)) are independent of composition; this assumption should be valid for dilute mixtures. The group G is a measure of the ability of the reaction to generate buoyancy and has units of frequency; in fact, $1/|G|$ is the time scale for buoyancy change in the plume caused by the chemical reaction. When G is positive, the reaction causes the buoyancy flux in the plume to increase. Combining (2.13) and (2.14), the relative change of the

fluxes of A and buoyancy in the plume owing to reaction is given by

$$\frac{\mathrm{d}(F_A/F_{A0})}{\mathrm{d}(B/B_0)} = \frac{3k\nu_A}{R}\frac{1}{G}. \tag{2.16}$$

Hence, when $|G| \gg 3k\nu_A/R$, the change in the flux of A in the plume is very small compared to the change in buoyancy flux. This means that the consumption of A by reaction is small, so that $F_A \approx F_{A0}$ in (2.13), that is, the mass flux of A is constant in the plume, and thus the balance for A in (2.14) is not required. Physically, this represents a situation where the buoyancy generated by reaction is large but the reaction rate is small. Such would occur when the reaction is strongly exothermic or involves a large change in density, for example, due to a phase change. We shall see later that our experiments in § 5 and the application to CO_2 sequestration in § 7 both satisfy this criterion. The limit of negligible consumption of reactant is in fact a common approximation in many problems involving chemical reaction, for example, in the modelling of combustion processes (Fairlie & Griffiths 2001; Liu *et al.* 2008). With this assumption, (2.13) simplifies to

$$\frac{\mathrm{d}B}{\mathrm{d}z} = -N^2 Q + \frac{1}{\gamma} G B_0 \frac{Q}{M}. \tag{2.17}$$

If we neglect further the effects of droplet coalescence or breakup in the plume, then $F_{A0}/F_A = (R_0/R)^3$, and the assumption of negligible consumption of A is equivalent to that of negligible change of the size of the droplets. In this case, G is constant in the plume. The behaviour of the plume is now described by the three ordinary differential equations (2.11), (2.12) and (2.17).

2.3. *Dimensionless plume equations*

Equations (2.11), (2.12) and (2.17) may be non-dimensionalized using

$$\hat{Q} = \frac{Q}{Q_s}; \quad \hat{M} = \frac{M}{M_s}; \quad \hat{B} = \frac{B}{B_0}; \quad \hat{z} = \frac{z}{L}. \tag{2.18}$$

When reaction is the dominant mechanism changing the plume buoyancy, the following scales can be derived:

$$Q_s = \left(8\pi\alpha^2\gamma^{-1}\right)^{1/4} B_0^{3/4} |G|^{-5/4}, \tag{2.19a}$$

$$M_s = \gamma^{-1} B_0 |G|^{-1}, \tag{2.19b}$$

$$L = \left(8\pi\alpha^2\gamma^{-1}\right)^{-1/4} B_0^{1/4} |G|^{-3/4}. \tag{2.19c}$$

The length scale L gives an indication of the distance over which significant buoyancy flux has been generated in the plume through reaction. Using these scales, the governing equations (2.11), (2.12) and (2.17) reduce to their simplest form:

$$\frac{\mathrm{d}\hat{Q}}{\mathrm{d}\hat{z}} = \hat{M}^{1/2}, \tag{2.20a}$$

$$\frac{\mathrm{d}\hat{M}}{\mathrm{d}\hat{z}} = \frac{\hat{B}\hat{Q}}{\hat{M}}, \tag{2.20b}$$

$$\frac{\mathrm{d}\hat{B}}{\mathrm{d}\hat{z}} = -\left(\frac{N}{G}\right)^2 \hat{Q} + \frac{\hat{Q}}{\hat{M}}\frac{G}{|G|}. \tag{2.20c}$$

Regime I: Reaction-dominant ($|G| \gg N$)

$$M = M_0 + \frac{1}{2}\frac{B_0}{\gamma G}\left[\left(\frac{B}{B_0}\right)^2 - 1\right] \tag{3.1}$$

$M_0 \ll \dfrac{B_0}{\gamma|G|}$

$$Q^2_{B=0} = Q_0^2 + \frac{3\pi}{8}(\pi\alpha^2\gamma^{-1})^{1/2}B_0^{3/2}|G|^{-5/2} \quad \text{for negative } G \tag{3.2}$$

$$Q^2_{M=0} = Q_0^2 + \frac{3\pi}{4}(\pi\alpha^2\gamma^{-1})^{1/2}B_0^{3/2}|G|^{-5/2} \quad \text{for negative } G \tag{3.3}$$

$M_0 \gg \dfrac{B_0}{\gamma|G|}$

$$Q^2 = Q_0^2 + \gamma(32\pi\alpha^2)^{1/2}\left(\frac{B}{B_0} - 1\right)M_0^{3/2}G^{-1} \tag{3.4}$$

$$z_{B=0} = (2\pi\alpha^2\gamma^{-2})^{-1/4}M_0^{1/4}|G|^{-1/2} \quad \text{for negative } G \tag{3.5}$$

$$z_{M=0} = \gamma(2\pi\alpha^2)^{-1/4}M_0^{3/4}B_0^{-1/2} \quad \text{for negative } G \tag{3.6}$$

Regime II: Stratification-dominant ($|G| \ll N$)

$$M^2 = M_0^2 - \frac{1}{\gamma N^2}(B^2 - B_0^2) \tag{3.7}$$

$M_0 \ll \dfrac{B_0}{\gamma^{1/2}N}$

$$Q^2_{B=0} = Q_0^2 + \frac{\pi^{1/2}\Gamma(1/4)}{3\Gamma(3/4)}\left(8\pi\alpha^2\gamma^{-1/2}\right)^{1/2}B_0^{3/2}N^{-5/2} \tag{3.8}$$

$$Q^2_{M=0} = Q_0^2 + \frac{2\pi^{1/2}\Gamma(1/4)}{3\Gamma(3/4)}(8\pi\alpha^2\gamma^{-1/2})^{1/2}B_0^{3/2}N^{-5/2} \tag{3.9}$$

$M_0 \gg \dfrac{B_0}{\gamma^{1/2}N}$

$$Q^2 = Q_0^2 + (32\pi\alpha^2)^{1/2}(B_0 - B)M_0^{1/2}N^{-2} \tag{3.10}$$

$$z_{B=0} = (2\pi\alpha^2)^{-1/4}B_0^{1/2}M_0^{-1/4}N^{-1} \tag{3.11}$$

$$z_{M=0} = (2\pi\alpha^2\gamma^{-2})^{-1/4}M_0^{1/4}N^{-1/2} \tag{3.12}$$

TABLE 1. Analytical solutions for the reaction-dominant and stratification-dominant regimes.

The boundary conditions for these equations are

$$\hat{Q}_0 = \frac{Q_0}{Q_s}; \quad \hat{M}_0 = \frac{M_0}{M_s}; \quad \hat{B}_0 = 1 \text{ at } \hat{z} = 0. \tag{2.21a,b,c}$$

The plume dynamics therefore depends on the magnitudes of the three non-dimensional groups

$$\hat{Q}_0 \sim \frac{Q_0\,|G|^{5/4}}{B_0^{3/4}}, \quad \hat{M}_0 \sim \frac{M_0\,|G|}{B_0} \text{ and } \frac{N}{G}. \tag{2.22a,b,c}$$

If $N/G = 0$, the behaviour of the plume depends on the magnitudes of (2.22*a*,*b*), as well as on the sign of G. Thus the dynamics of a pure plume with chemical reaction rising in a uniform environment is determined by the sign of G only. This is an important conclusion which we shall explore in the laboratory experiments in §§ 5 and 6.

3. Analytical results

When the effects of buoyancy generated by chemical reaction on the dynamics of the plume are much larger than those caused by stratification, that is, $|G| \gg N$, some analytical solutions to (2.20) and (2.21) may be obtained. These solutions are summarized in table 1. Relation (3.1) shows that, when $G < 0$, both the maximum momentum flux and the buoyancy flux at the level of zero momentum depend on the magnitude of the group $B_0/(\gamma|G|)$ but are independent of the initial flow rate in the plume. For strong jet-like behaviour near the source, that is, $\hat{M}_0 \gg 1$ or

$M_0 \gg B_0/(\gamma|G|)$, the level of neutral buoyancy is proportional to $M_0^{3/4}|G|^{-1/2}$ (see (3.5)) and the level of zero momentum is proportional to $M_0^{3/4}B_0^{-1/2}$ (see (3.6)). At these levels, the flow rates in the jet can be calculated from relation (3.4). For strong plume-like behaviour near the source, that is, $\hat{M}_0 \ll 1$ or $M_0 \ll B_0/(\gamma|G|)$, the flow rates in the plume at the levels of neutral buoyancy and zero momentum grow proportionally to $B_0^{3/4}|G|^{-5/4}$ and are given by (3.2) and (3.3), respectively.

For comparison, we also show in table 1 the solutions to (2.20) and (2.21) in the limit of very strong stratification, $|G| \ll N$. We note that the structures of the solutions for strong stratification differ from the corresponding ones for strong reaction because of the different form of the two terms on the right-hand side of the equation for the buoyancy flux (2.20*c*). For strong jet-like behaviour near the source, that is, $M_0 \gg B_0/(\gamma^{1/2}N)$, the level of neutral buoyancy is given by (3.11) and the level of zero momentum by (3.12). It is worth pointing that for a jet rising in a strong stratification, the level of neutral buoyancy depends on the initial buoyancy flux. This contrasts with the case of a jet with strong chemical reaction, for which the level of neutral buoyancy is independent of the initial buoyancy flux (cf. (3.5)). For strong plume-like behaviour near the source, that is, $M_0 \ll B_0/(\gamma^{1/2}N)$, the flow rates in the plume at the levels of neutral buoyancy and zero momentum grow proportionally to $B_0^{3/4}N^{-5/4}$and are given by (3.8) and (3.9), respectively.

In the next section, we shall compare some of these analytical predictions with the full numerical simulations of (2.20) and (2.21).

4. Numerical results

The governing equations (2.20) and (2.21) were solved numerically using *Mathematica*, for a pure plume with a range of N and G. In addition to calculating the volume, momentum and buoyancy fluxes in the plume as a function of ascent distance, we also show its width b and centreline velocity w_c. The non-dimensional parameter

$$\Gamma = (8\pi)^{-1/2}\frac{5}{4\alpha\gamma^2}\frac{BQ^2}{M^{5/2}} = \frac{5}{4}\frac{\hat{B}\hat{Q}^2}{\hat{M}^{5/2}} \tag{4.1}$$

indicates whether the plume is forced or jet-like ($\Gamma < 1$), pure ($\Gamma = 1$) or lazy ($\Gamma > 1$). It is similar to that used by Hunt & Kaye (2005) but has been extended here to include the turbulent transport factor γ. Since our model considers a pure plume at the source, the magnitude of Γ shows the deviation from the pure plume behaviour caused by reaction and/or environmental stratification.

In figure 1, we present the results for a pure plume issuing from a point source and rising in a uniform environment. When G is positive (solid line), the chemical reaction generates buoyancy as the plume ascends. As a result, the buoyancy flux increases above its value at the source. The flow rate and momentum fluxes also increase with height, as expected, and the plume motion is unbounded. The plume spreads nearly linearly with height, but in spite of this expansion the velocity decreases very slowly at large distances from the source. The parameter Γ increases slightly from the inert plume value of one at the source, showing that reaction caused the plume to become marginally 'lazy'. In contrast, when G is negative (dashed line), the buoyancy flux in the plume decreases due to the reaction. Since our model assumes that the flux of reactant is approximately constant (c.f. (2.16)), the reactant is never depleted and hence the motion is always bounded. The plume behaves as 'forced' and Γdecreases

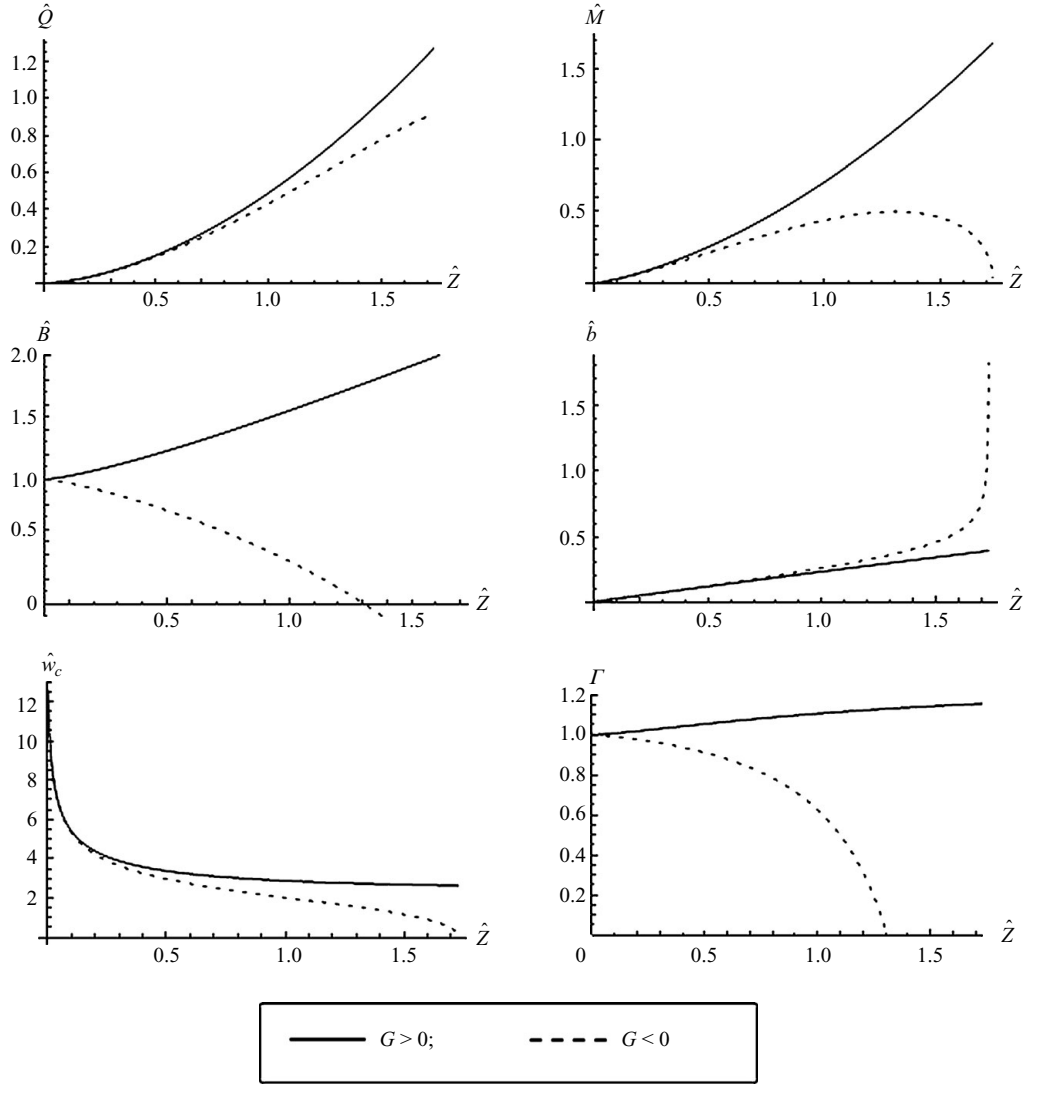

FIGURE 1. Effects of the sign of the reaction parameter G on the behaviour of a plume rising in an environment of uniform density. Shown are the non-dimensional flow rate, specific momentum flux, specific buoyancy flux, plume radius, centreline velocity and parameter Γ as a function of height.

to zero, as the plume reaches its neutral buoyancy level at

$$z_{B=0} = 1.31\ (8\pi\alpha^2\gamma^{-1})^{-1/4} B_0^{1/4} |G|^{-3/4}. \tag{4.2}$$

At this level, the flow rate is given by

$$Q_{B=0} = 0.70\ (8\pi\alpha^2\gamma^{-1})^{1/4} B_0^{3/4} |G|^{-5/4}. \tag{4.3}$$

Above the level of neutral buoyancy, the momentum flux decreases until it eventually reaches zero at

$$z_{M=0} = 1.73\,(8\pi\alpha^2\gamma^{-1})^{-1/4} B_0^{1/4} |G|^{-3/4}. \tag{4.4}$$

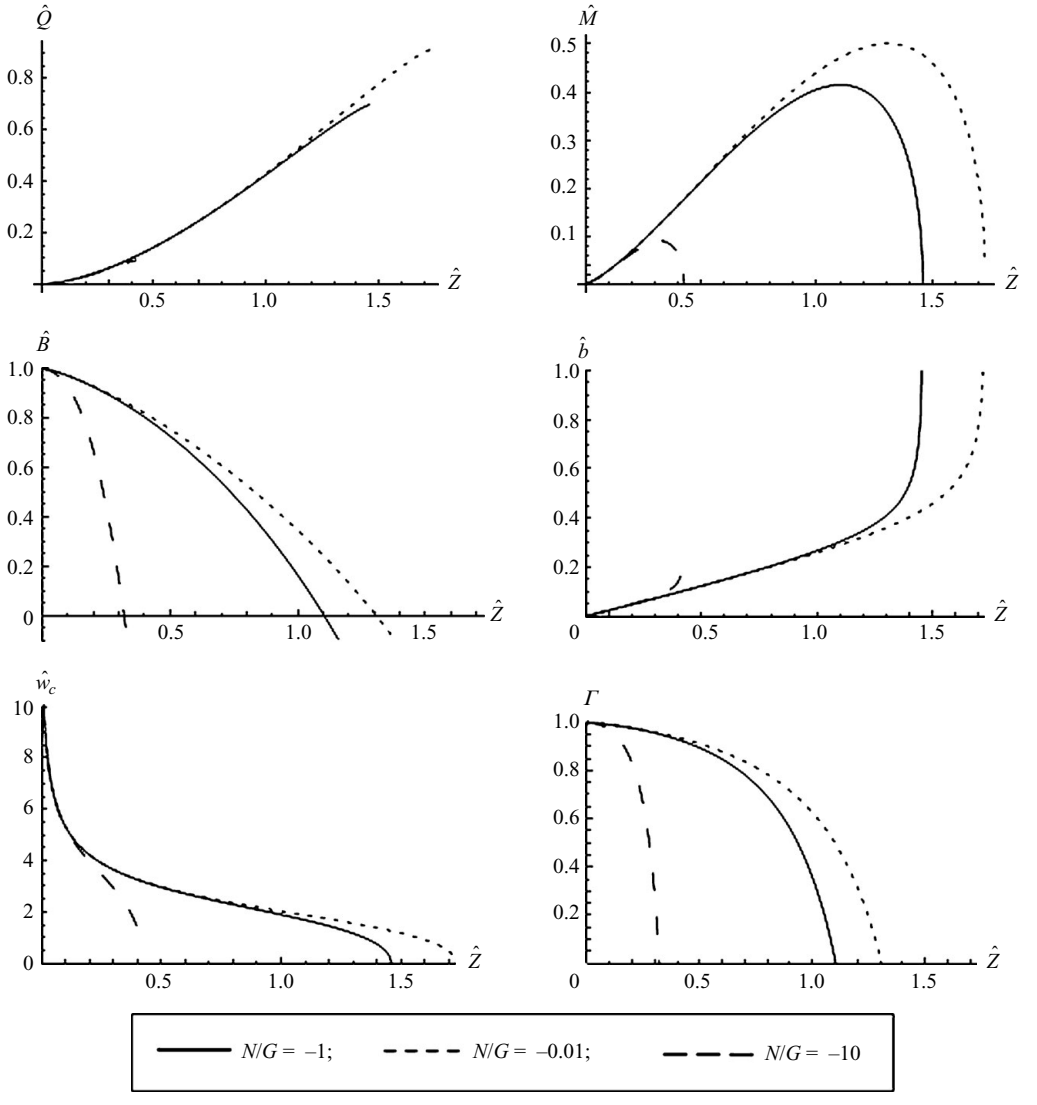

FIGURE 2. Effects of the group N/G on the behaviour of a plume in which reaction decreases buoyancy (negative G). Shown are the non-dimensional flow rate, specific momentum flux, specific buoyancy flux, plume radius, centreline velocity and parameter Γ as a function of height.

At this point the radius increases abruptly. In the region in between the levels of neutral buoyancy and zero momentum, some phase separation should occur because the droplet slip velocity becomes larger than the plume velocity. Also, the assumption of a constant entrainment coefficient becomes dubious. The model developed in this paper is therefore valid only up to the neutral buoyancy level.

Figure 2 shows the effects of the group N/G on the behaviour of a pure plume when reaction decreases buoyancy. The long-dashed line shows the effects of strong stratification. The short-dashed line shows the effects of very strong reaction; these results are similar to those for a uniform environment and negative G, seen in figure 1. The solid line shows the combined effects of stratification and reaction. The flow rate $\hat{Q}$ has little sensitivity to N/G. It is only above the neutral buoyancy level,

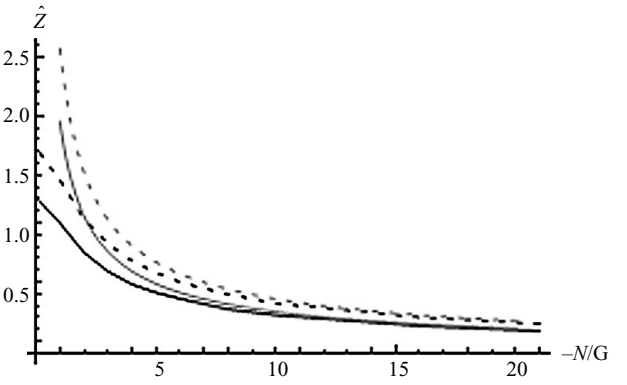

FIGURE 3. Levels of neutral buoyancy (solid black line) and zero-momentum (dashed black line) as a function of the group N/G for a plume in which reaction depletes buoyancy (negative G); note that the motion of plume is bounded by reaction when $N = 0$. Also shown are levels of neutral buoyancy (solid grey line) and zero-momentum (dashed grey line) for an inert plume; in this case, the motion of the plume is unbounded for $N = 0$.

when $\hat{M}$ changes sharply, that N/G has a slight effect on $\hat{Q}$. The magnitudes of the flow rate and of the momentum flux at the neutral buoyancy level, for strong stratification and strong reaction, agree with the predictions in table 1. For example, when G is large, the maximum momentum attained is expected to be $\hat{M} = 1/2$ from (3.1), which is in agreement with the short-dashed line in figure 2(b). As the negative buoyancy generated by reaction increases, that is, $|G|$ becomes larger, the non-dimensional buoyancy flux decreases more slowly with non-dimensional height (figure 2c). This is only an apparent effect due to non-dimensionalization. In fact, the neutral buoyancy level decreases sharply with G. In the limit of very strong stratification, the numerical results in figure 2(c) suggest that the neutral buoyancy level is given by $z_{B=0} = 1.955(8\pi\alpha^2\gamma^{-1})^{-1/4}B_0^{1/4}N^{-3/4}$. When $\gamma = 1$, this result is similar to the prediction of Morton *et al.* (1956) for the neutral buoyancy level of an inert, single-phase plume in a stratified environment.

Figure 3 shows how the levels of neutral buoyancy (solid black line) and zero momentum (dashed black line) decrease with the magnitude of N/G when G is negative. The levels of neutral buoyancy (solid grey line) and zero momentum (dashed grey line) for an inert plume are also shown; when $\gamma = 1$, these results coincide with the solutions of Morton *et al.* (1956), namely $z_{B=0} = 1.955(8\pi\alpha^2)^{-1/4}B_0^{1/4}N^{-3/4}$ and $z_{M=0} = 2.570(8\pi\alpha^2)^{-1/4}B_0^{1/4}N^{-3/4}$. For $N = 0$, the flow in the reactive plume is bounded by the effect of chemical reaction, whilst for $|N/G| > 10$ the flow is controlled by stratification in the ambient fluid and reaction has little effect, that is, the plume behaves as an inert one.

Figure 4 illustrates the effects of the sign and magnitude of G on the plume dynamics in a stratified environment. As seen previously for a uniform environment (cf. figure 1), the flow rate in the plume in a stratified environment has also little sensitivity to the value of N/G. For the dashed lines, G is positive, that is, the reaction generates buoyancy and hence the buoyancy flux increases above that at the source. However, above some height, the flow rate becomes sufficiently large for the effects of entrainment to dominate over those due to reaction and, as a result, the buoyancy flux starts decreasing. The maximum buoyancy flux occurs at the level at which $\hat{M} = (N/G)^{-2}$. The width of the plume is approximately equal in all three cases shown, up to the level of neutral buoyancy, where the plume spreads radially. When

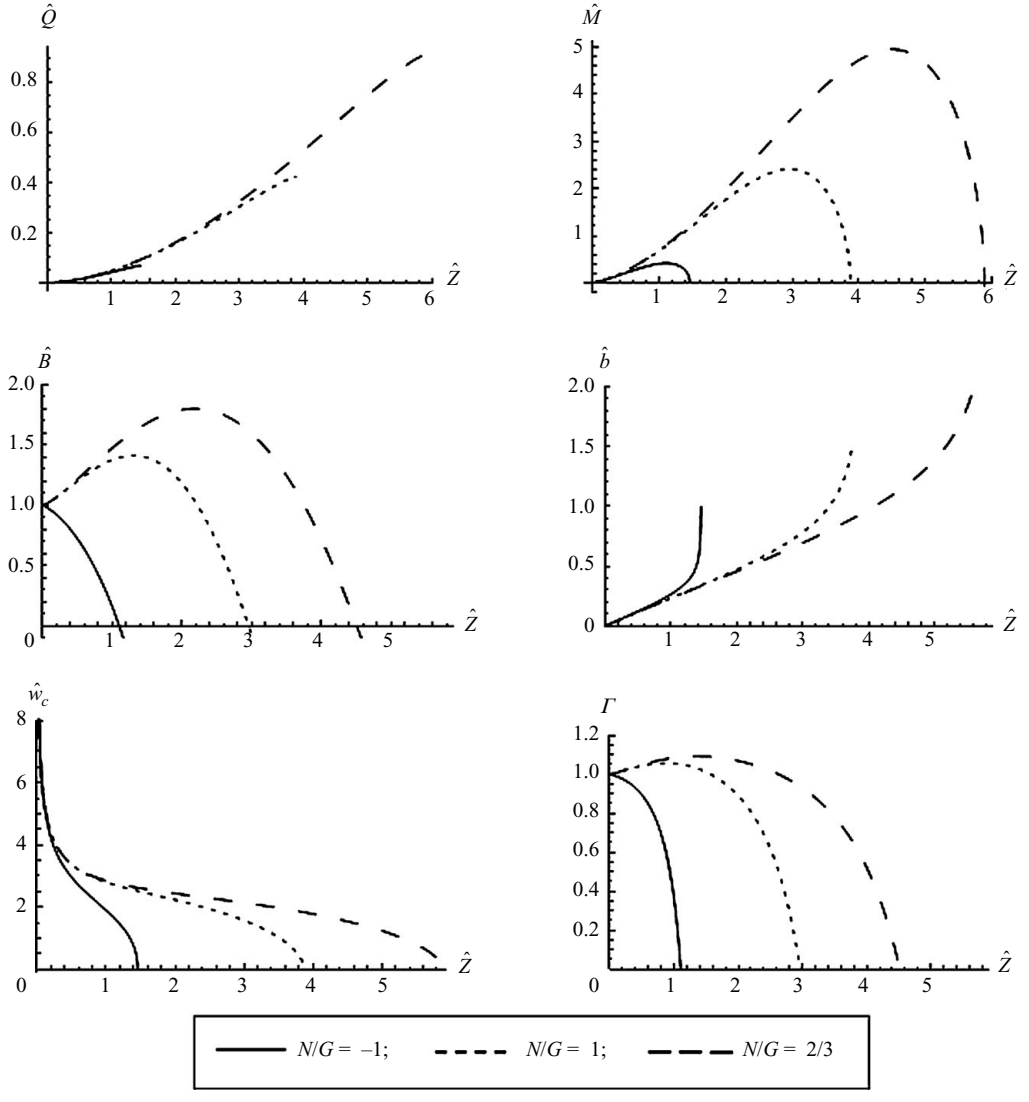

FIGURE 4. Effects of the sign of G on the behaviour of the plume rising in a stratified environment. Shown are the non-dimensional flow rate, specific momentum flux, specific buoyancy flux, plume radius, centreline velocity and parameter Γ as a function of height.

G is positive, Γ increases slowly from the pure plume value of one to a maximum, after which there is a strong decrease, that is, the plume behaves first as 'lazy' owing to reaction, but then becomes 'forced' owing to stratification.

Figure 5 shows the levels of neutral buoyancy (solid line), maximum momentum (short dash) and maximum buoyancy flux (long dash) as a function of N/G, when G is positive. The unbounded motion expected for the case $N = 0$ is clearly seen. As the effects of stratification become stronger compared to those of reaction, the entrainment of relatively heavy ambient fluid arrests the motion of the plume at decreasing levels.

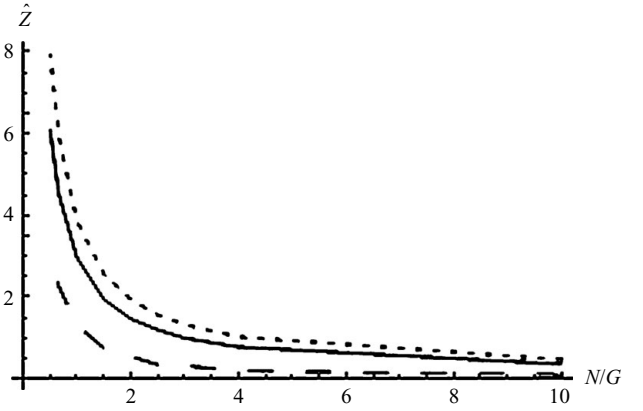

FIGURE 5. Levels of neutral buoyancy (solid line), zero-momentum (short dash) and maximum buoyancy flux (long dash) as a function of the group N/G for a plume in which reaction increases buoyancy (positive G). Note that the motion of the plume is unbounded when $N \to 0$.

5. The experiments

Conducting laboratory experiments to complement the theory developed above posed a number of difficulties. These include: (i) identifying a heterogeneous chemical reaction that causes significant and measurable differences in the plume dynamics compared to that in a non-reactive plume on the laboratory scale; (ii) also, the reaction has to be slow enough compared to the time scale for turbulent mixing, that is, the Damkohler number has to be sufficiently small (see § 2); (iii) the reaction rate should be varied to investigate a range of conditions, in particular a range of the magnitude of group G, but still satisfying the constraints above. These difficulties limited the experimental programme. The chemical system chosen involved calcium carbonate particles in the plume and an aqueous solution of hydrochloric acid in the environment. For safety reasons, the latter precluded the use of the double-bucket system to create a density stratified environment. As a result, only reactive plumes in a uniform environment were studied experimentally. Although the experimental programme is somewhat limited, the results presented below constitute the first study of the dynamics of a plume with heterogeneous chemical reaction.

The plume was formed by releasing small calcium carbonate particles at the top of an aqueous solution of hydrochloric acid, where they descend and react to form tiny bubbles of CO_2, according to

$$2H^+(aq) + CaCO_3(s) \rightarrow H_2O + CO_2(g) + Ca^{2+}(aq). \tag{5.1}$$

The acidic environment had uniform density and was contained in a Perspex tank with a square cross-section of 20 cm $\times$ 20 cm and height 40 cm. The calcium carbonate particles were of grade Solvay SOCAL and subsequently sieved between 125 and 300 μm sieve gratings to obtain the mean diameter 220 μm. The buoyancy flux at the source was determined by the flow rate and density of the $CaCO_3$ particles relative to that of the liquid environment. The buoyancy change in this plume occurs as a result of the formation of the CO_2 bubbles. The diameter of the bubbles formed during reaction was estimated to be smaller than 50–100 μm.

The reaction rate was determined by measuring the rate of CO_2 production within a flask containing the acidic solution and $CaCO_3$ particles, for different values of initial liquid pH. The rate of CO_2 production was measured for varying intensities of

Experimental conditions	Q_{p0} (cm^3 s^{-1})	B_0 (cm^4 s^{-3})	pH	G (s^{-1})
1. Strong reaction	1.11	1510	1.72	−1.20
2. Intermediate reaction	1.11	1510	2.02	−0.78
3. No reaction	1.11	1510	7	0

TABLE 2. Plume and reaction parameters for the experiments using PIV: particle flow rate Q_{p0} and specific buoyancy flux B_0, as well as pH of the tank solution and reaction frequency G.

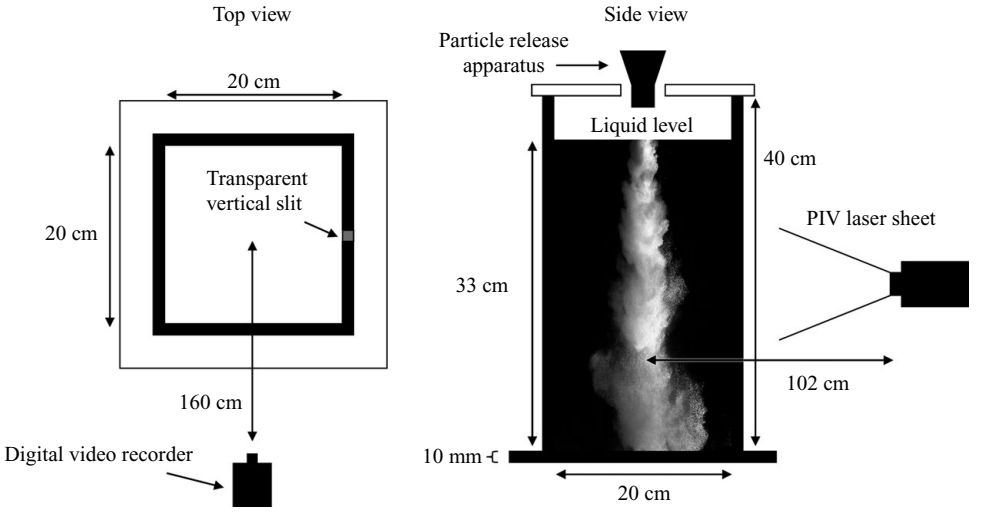

FIGURE 6. Schematic of the experimental set-up.

mixing in the flask. It was found that the reaction rate is independent of the intensity of mixing provided the degree of turbulence is sufficient to keep the particles in suspension. In this case, the reaction is limited by the acidity of the fluid surrounding the particles.

A schematic of the experimental set-up is shown in figure 6. A reservoir in the shape of a funnel, placed directly above and in the middle of the Perspex tank, was filled with $CaCO_3$ particles. Throughout an experiment, the height of particles in this reservoir remained large enough to yield a steady flow of particles. The funnel exit was placed at least 3–4 cm above the liquid surface. Table 2 summarizes the range of plume and reaction parameters for which experiments were performed. For each experimental condition, up to four nominally identical experiments were performed. In the experiments with reaction, $3k\nu_A/R \sim 10^{-4}$–$10^{-3}\,\mathrm{s}^{-1}$ and $G \sim 0.78$–$1.2\,\mathrm{s}^{-1}$, this satisfying the criterion $|G| \gg 3k\nu_A/R$ (cf. (2.16)) for negligible consumption of calcium carbonate and allowing the approximation that the particle size remains constant during reaction. We also estimate the Damkohler number in the plume to be in the range $Da = (\nu/\varepsilon)^{1/2}k/R \sim 10^{-2}$–$10^{-1}$, so that the assumption of slow reaction compared to turbulent mixing is valid.

The velocity field in the plume was measured using the technique of PIV. The calcium carbonate particles served the dual purpose of both the source of buoyancy and of tracer particles for the PIV. Indeed, the slip velocity of these particles (~ 0.7–$1\,\mathrm{cm\,s}^{-1}$) was much smaller than the plume velocity ($\sim 10\,\mathrm{cm\,s}^{-1}$). Also, the relaxation time for the particles to adjust to changes in velocity in the plume was of the order of 1 ms, which is much smaller than the turbulence integral time, typically of

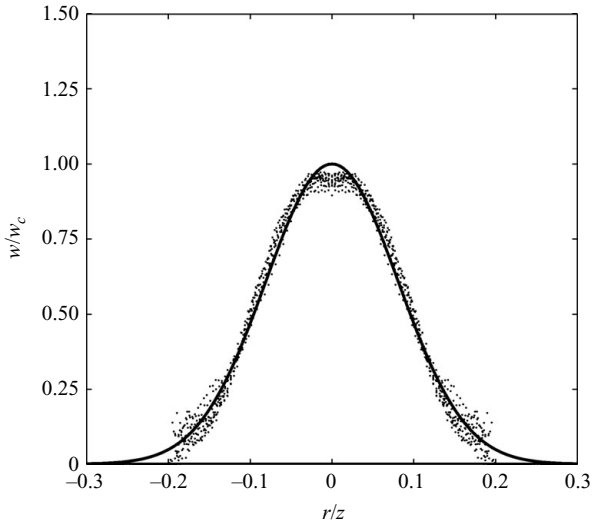

FIGURE 7. Time-averaged axial velocity w normalized by the centreline value w_c as a function of the normalized plume radius (r/z) for an inert plume with calcium carbonate particles. The solid line is the Gaussian best-fit to the experimental data points. The profile has been mirrored about the plume centreline, based on PIV measurements for the half of the plume with highest signal to noise ratio (i.e. closest to the light source).

0.1–0.5 s, so the particles behaved as neutrally buoyant. Image acquisition commenced once a pseudo steady-state flow had been established in the plume, typically 15 s after the injection of particles started. A 532 nm Nd:YAG dual cavity laser was used to illuminate the plume using a sequence of rapid double pulses of light, where pulse pairs were created with a frequency of 4 Hz. The separation time between each pulse within a pair was 2 ms, and typical particle displacement between frames was 1–3 pixels for this pulse separation interval. We used a 12-bit greyscale PCO Sensicam CCD camera with a resolution of 1280×1024 pixels to record images created by each pulse of laser light. Laser pulse intensity was set experimentally to maximize incident light intensity, while still avoiding any large-scale highlight clipping upon measurement of this light at the CCD. The camera was positioned so that its field of view covered an area within the plume of 24.2 cm in height by 19.4 cm in width. This imaging height was significantly smaller than the height of the light sheet, which ensured an approximately uniform distribution of laser intensity. The PIV data was averaged to obtain the highest resolution, with as few as possible erroneous vectors. The time averaging was performed over a period of 15 s. Additionally, spatial averaging was performed in the vertical and horizontal directions on the time-averaged PIV data in order to reduce noise. The vertical and horizontal resolutions were of 6.05 mm and 0.76 mm, respectively, although spatial smoothing was present for features smaller than 12.1 mm and 1.52 mm in the vertical and horizontal directions, respectively, due to a 50 % overlap of the PIV interrogation cells.

The experimental procedure and measurement techniques were validated by comparing the radial profiles of axial velocity for the particle-laden plume without reaction, shown in figure 7, with previously published data for a single phase, buoyant plume by Papanicolaou & List (1988). The Gaussian best-fit (solid line) has a $1/e$ radius of 0.110 in figure 7, whereas the data of those authors suggest a value of 0.105; the two data sets are in agreement within the experimental error. Figure 7 exhibits flattening near the plume centreline due to two effects. For the small plume

widths near the source, the PIV resolution and spatial smoothing become significant compared to the typical 5–10 mm plume radius. At larger plume widths, the turbulence integral time is larger, causing greater uncertainty in the time-averaged flow and in the location of the plume centreline.

6. Comparison of experimental and numerical results

In this section, we present the time-averaged results obtained using the PIV technique and compare them with our numerical predictions. Figure 8 presents the radial profiles of vertical velocity in an inert plume and in a reactive plume, for three different vertical positions. In the inert plume, the centreline velocity first increases slightly and then remains almost constant, with vertical distance, whilst the plume widens due to entrainment. In the reactive plume, the centreline velocity is smaller than that in the inert plume and decreases with height, because of the opposing buoyancy produced by the reaction. Up to the level of neutral buoyancy ($z \sim 100$–110 mm), the velocity distribution is approximately Gaussian in the reactive plume. However, above this level, the velocity profile becomes flattened and phase separation occurs: particle-laden fluid descends in the centre of the plume, whilst bubble rich, buoyant fluid ascends at its periphery. This reverse flow at the edge of the plume is clearly seen in figure 8(c).

Figure 9 shows the volume and momentum fluxes as a function of vertical position, for the inert and reactive plumes as detailed in table 2. These fluxes were obtained from integration of the radial velocity distribution obtained with the PIV. The error bars take into account (i) variation between repeat experiments, (ii) the error associated with the averaging of the turbulent field over a finite time compared to the turbulent integral time scale and (iii) variation caused by the size of the PIV interrogation area (8×8 pixels versus 32×32 pixels). As expected, for the inert plume, the volume and momentum fluxes increase with vertical distance. For intermediate reaction strength ($G = -0.78$), the effect of the chemical reaction, which generates opposing buoyancy, is to decrease the rate at which these fluxes increase. In fact, the momentum flux becomes constant above 120 mm. In the case of strong reaction ($G = -1.2$), the volume and momentum fluxes actually decrease above the neutral buoyancy level, at $z \sim 100$–110 mm. This decrease occurs because of phase separation and the associated reverse flow at the edge of the plume, as seen previously in figure 8(c).

In figure 10, we present the plume radius and the centreline velocity as a function of vertical position. These plume properties were calculated from the measured volume and momentum fluxes and assuming a radial Gaussian distribution for the vertical velocity. Above the neutral buoyancy level, these properties should be seen with some caution since the velocity profile deviates from Gaussian due to phase separation (cf. figure 8c). Our measurements suggest that reaction has little effect on the plume radius. However, the plume velocity for strong reaction is clearly smaller than in the cases of no reaction and intermediate reaction strength. These experimental results suggest that the chemical reaction decreases the volume and momentum fluxes in the plume by decreasing the velocity but not by reducing the plume radius. This behaviour is in qualitative agreement with the numerical predictions in figure 1, which showed a very small change in plume radius but a large reduction in velocity when G becomes negative.

Figure 11 presents a comparison between the experimental measurements and the theoretical predictions for the volume and momentum fluxes in an inert plume. The theoretical predictions include those for a pure plume and for a finite source with initial volume and momentum fluxes as measured by the PIV. This comparison is

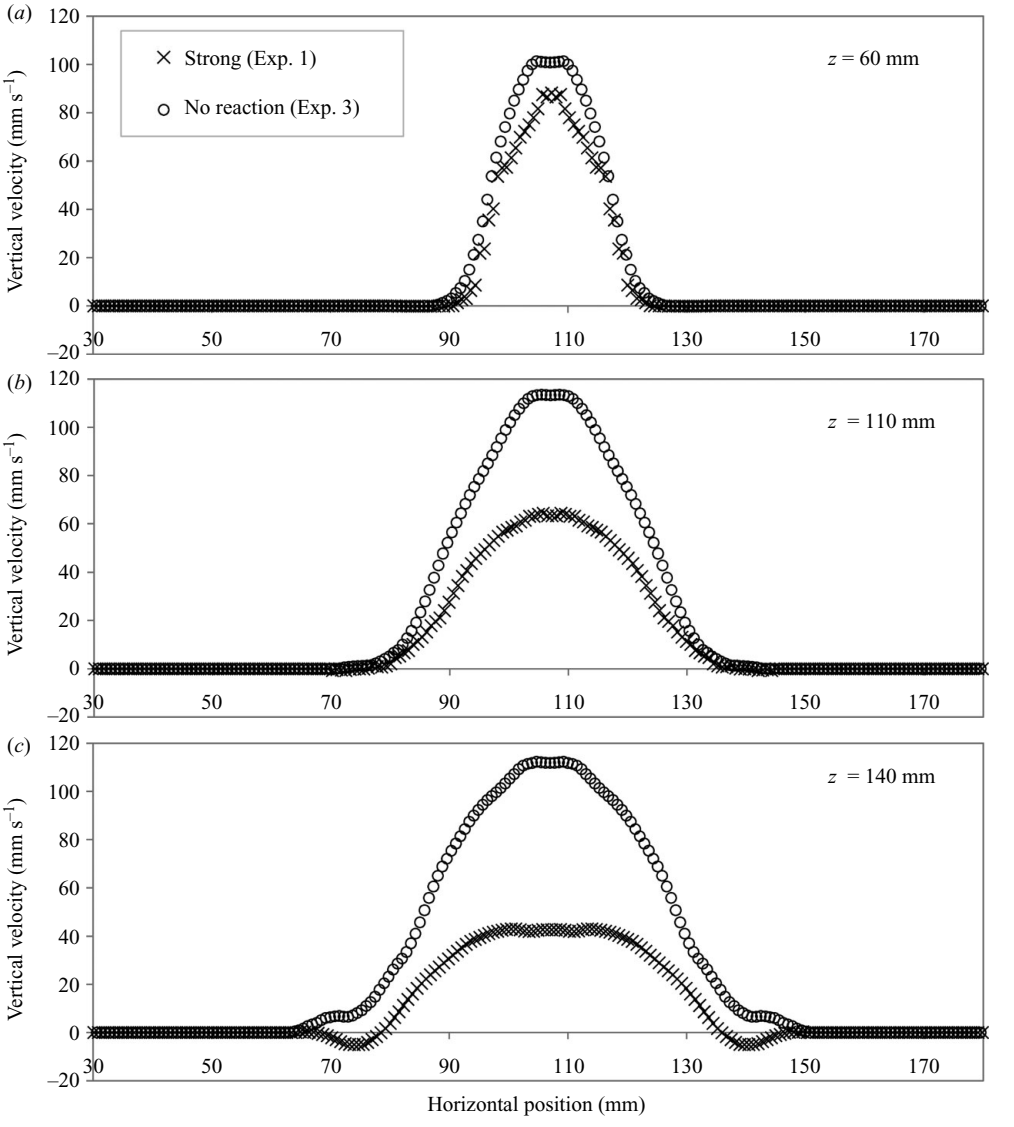

FIGURE 8. Radial profile of time-averaged vertical velocity for a plume with no reaction (○) and a plume with strong reaction (X) at vertical positions: (*a*) 60 mm, (*b*) 110 mm and (*c*) 140 mm, from the source. Profiles have been mirrored about the plume centreline, based on PIV measurements for the half of the plume with highest signal to noise ratio (i.e. closest to the light source).

made dimensionally because there is no natural length scale for a pure inert plume in a uniform environment. The flow rate and momentum fluxes are reasonably well predicted using an entrainment coefficient $\alpha = 0.11$ and a turbulent factor $\gamma = 1.4$. The predictions for the pure plume and for the finite source are very close, within the experimental error margin, indicating that the source fluxes in the experiments are sufficiently small to be neglected. An entrainment coefficient $\alpha = 0.11$ is well within the range measured by other authors. Indeed, α has been determined experimentally for single-phase plumes in a number of studies as summarized by Linden (2000). For Gaussian profiles, values in the range 0.08–0.11 are appropriate. For bubble plumes,

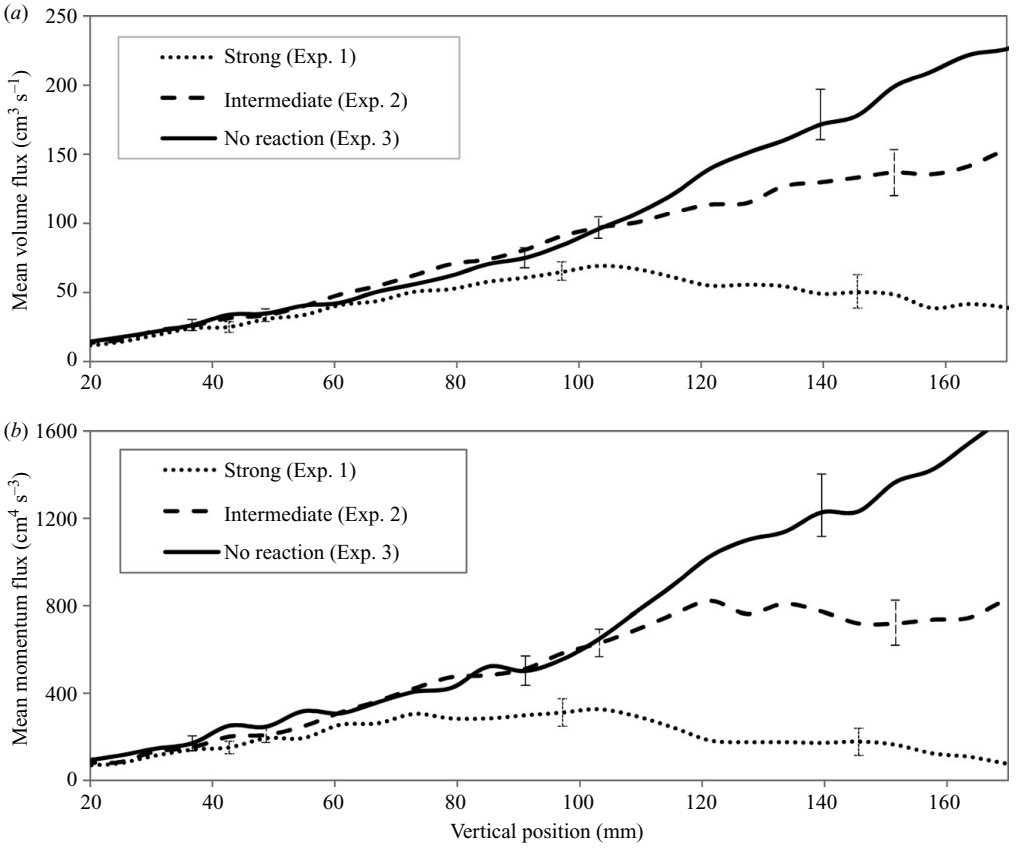

FIGURE 9. Measured (*a*) volume flux and (*b*) specific momentum flux as a function of vertical position in the plume for the three reaction rates detailed in table 2.

Milgram (1983) measured $\alpha \sim 0.10$–0.16 (Gaussian profiles) for his largest bubble Froude number. Also, experimental results for plumes of very small bubbles (Chen & Cardoso 2000) and plumes with very small particles (Zarrebini & Cardoso 2000) are consistent with $\alpha \sim 0.09$ (Gaussian profiles). The momentum flux is particularly sensitive to the value of γ, as seen by comparing the results for $\gamma = 1.4$ and $\gamma = 1.6$ in figure 11. A value of $\gamma = 1.4$ is well within the range measured by Milgram (1983) for bubble plumes. Figure 12 shows the plume radius and centreline velocity. Whilst the plume radius is well predicted by the theory, the predictions for the centreline velocity show a decrease with vertical position that is not observed experimentally. This discrepancy may however be partially explained by the experimental precision, as shown by the error bars. Additionally, we expect the PIV measurements to have low accuracy near the source of the plume, where particle concentrations are very large and spatial smoothing is significant (see § 5). We confirm again that the theoretical results for the pure plume are very close to those for the finite source, indicating that the source fluxes have only a small effect on the plume behaviour.

In figure 13, we show a comparison between experiments and theory for plumes with intermediate and strong chemical reaction. The results here are non-dimensionalized according to (2.18) and (2.19). The theoretical predictions include those for a pure plume and for a finite source with initial volume and momentum flux as measured by

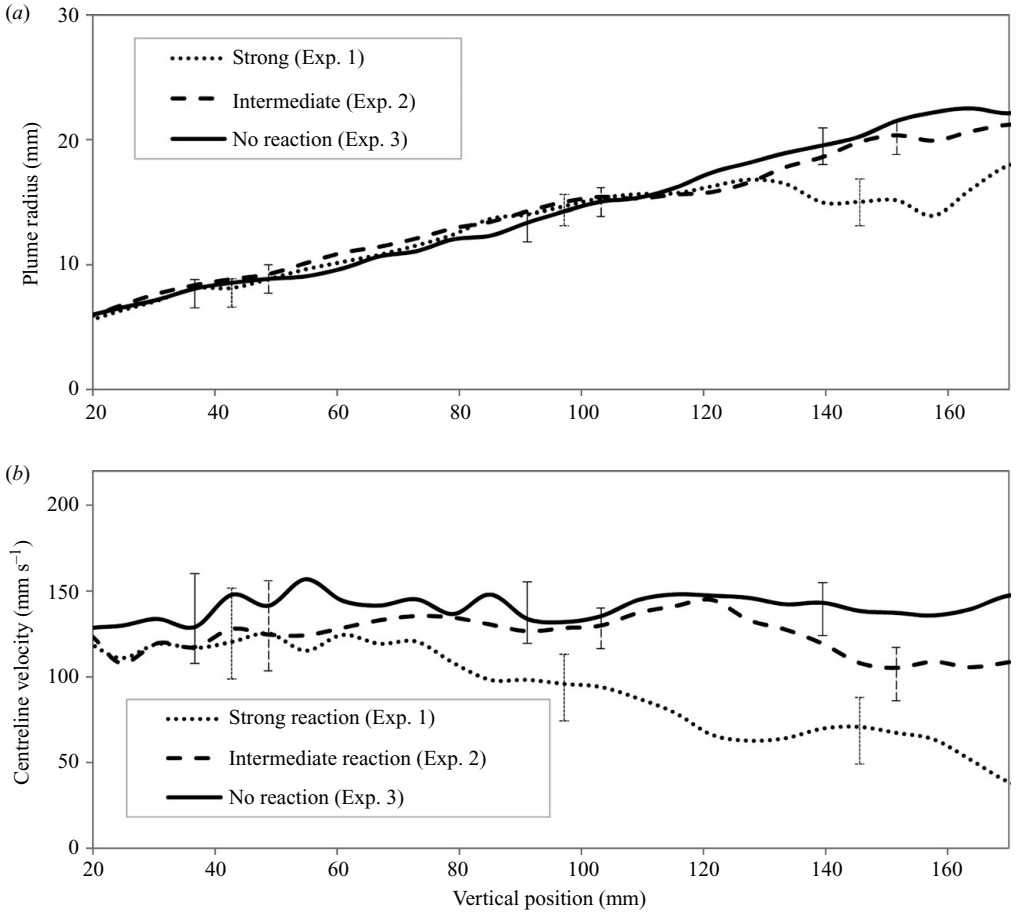

FIGURE 10. (*a*) Plume radius and (*b*) centreline velocity as a function of vertical position in the plume for the three reaction rates detailed in table 2. These plume properties were calculated from the measured volume and momentum fluxes assuming a radial Gaussian distribution of the vertical velocity.

the PIV. The entrainment coefficient was taken as $\alpha = 0.10$ and the turbulent factor as $\gamma = 1.4$, for the best agreement between experiments and theory. The theoretical prediction for the flow rate is in excellent agreement with the experimental results up to the level of neutral buoyancy, for both reaction strengths. Above this level, some phase separation occurs and the assumption of a constant entrainment coefficient is no longer valid, so the theory is unable to predict the decrease in flow rate seen for the strong reaction. The predictions and measurements for the momentum flux are also in good agreement for the reaction with intermediate strength. Although there is a noticeable difference between theory and experiment for the stronger reaction, it is of order of the error margin indicated by the error bars. The vertical position at which the momentum flux is maximum is also reasonably well predicted by the theory for both the cases of intermediate and strong reaction. As seen before for the inert plume, the predictions for the pure plume and for the actual finite source are close, so the effects of initial flow rate and momentum in the experiments are small.

The value of the entrainment coefficient for the reactive plumes, $\alpha = 0.10$, is slightly smaller than that used in figure 8 for the inert plume ($\alpha = 0.11$). However, a reduction

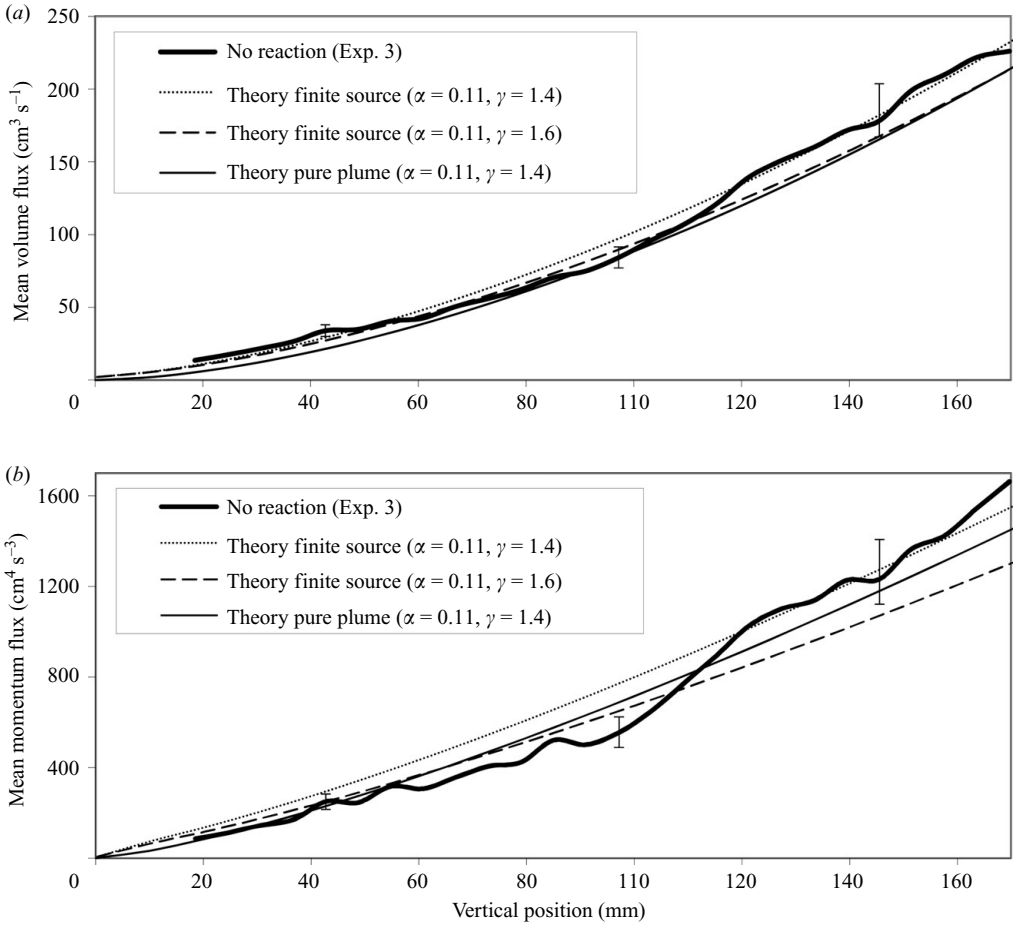

FIGURE 11. (*a*) Volume flux and (*b*) specific momentum flux as a function of vertical position for an inert plume. Comparison between experimental measurement and theoretical predictions.

in the entrainment coefficient when the chemical reaction reduces buoyancy might be expected. Indeed, it has long been suggested that the entrainment coefficient in a plume decreases when the local Richardson number is reduced (Priestly & Ball 1955) and that entrainment in plumes is larger than that in jets. More recently, the theoretical work by Kaminski *et al.* (2005) suggests that the entrainment coefficient in a plume depends not only on the local Richardson number but also on the shapes of the radial velocity and buoyancy profiles and their rate of change with height in the plume. Also, the experimental work by Carazzo, Kaminski & Tait (2006) has shown reduced entrainment in negatively buoyant jets. Nevertheless, the change in entrainment coefficient from the inert to the reactive plumes in our study is very small and therefore the assumption of a constant α up to the level of neutral buoyancy seems to be reasonable. The value of the turbulent factor $\gamma = 1.4$ used for the reactive plumes is the same as that for the inert plume. One might have anticipated that the bubbles formed during reaction might have contributed to increase γ, but perhaps their very small size, of the order of 50–100 μm, is responsible for their negligible effect on turbulent transport.

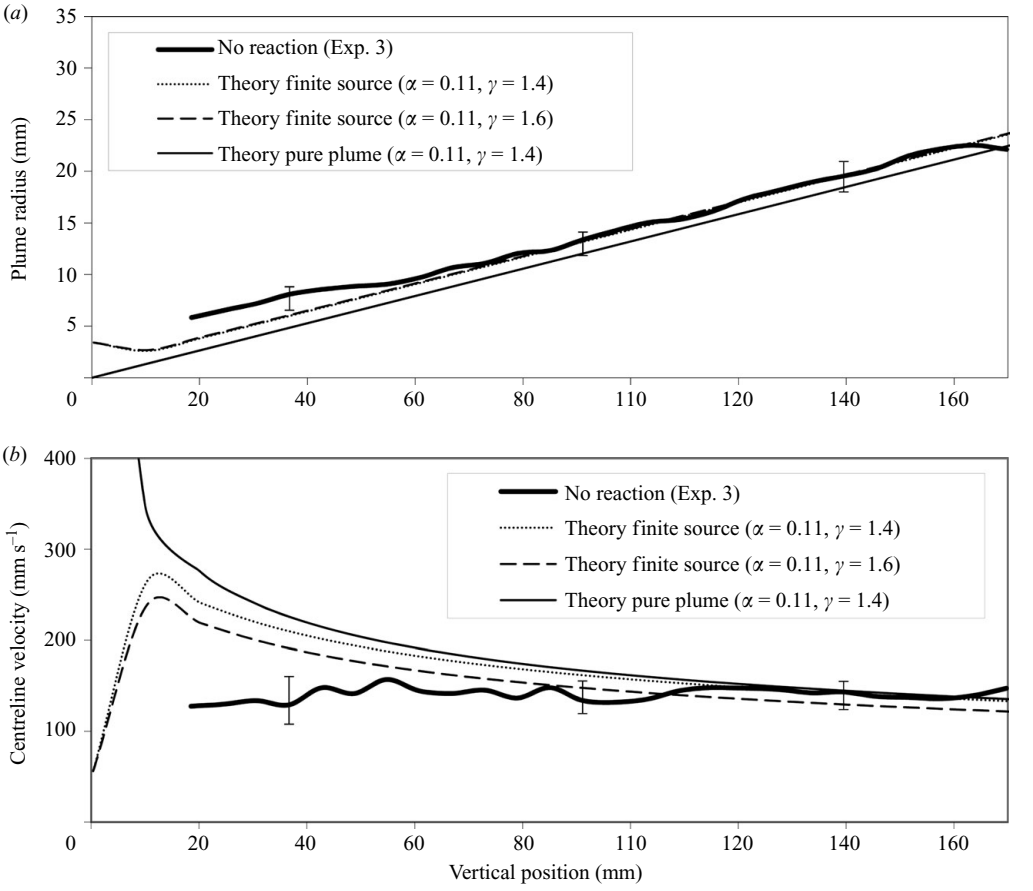

FIGURE 12. (*a*) Plume radius and (*b*) centreline velocity as a function of vertical position for an inert plume. Comparison between experimental measurement and theoretical predictions.

Figure 14 presents the non-dimensional plume radius and centreline velocity for the reactive plumes. As before, the plume radius is well predicted by the theory, but the centreline velocity shows a decrease with vertical position that is not observed experimentally. However, this discrepancy might be explained by the lower accuracy of the PIV measurements near the plume source (see § 5).

7. Application to a CO_2 release in the ocean

The direct injection of carbon dioxide into the ocean has been proposed to mitigate its influence on global climate change. Alternatively, an accidental release might occur if underground CO_2 used in enhanced oil recovery or sequestered in saline aquifers were to escape from reservoirs on the ocean floor (Metz *et al.* 2005). At typical depths of 1000 m, the ocean temperature is 2–10 °C, the pressure is ∼100 atm and the density of seawater is ∼1030 kg m^{-3}. At such temperatures and pressures, CO_2 is a liquid, with a density of ∼950 kg m^{-3}, and is only partially miscible in seawater. A deep ocean release of CO_2 would therefore form a rising plume of droplets, which gradually dissolve, and can react with water to form crystalline CO_2 hydrates at depths exceeding ∼450 m. Brewer *et al.* (2002) demonstrated that these hydrates envelop the CO_2 droplets and inhibit the dissolution of CO_2 in seawater. The heavier

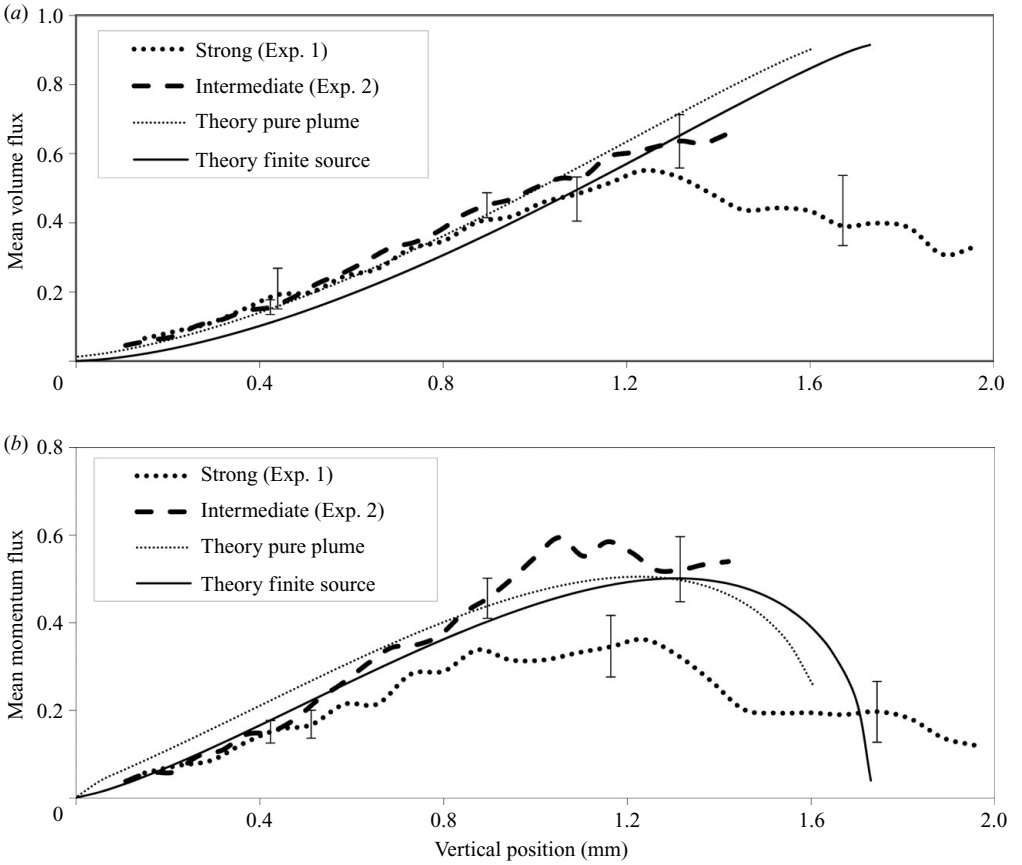

FIGURE 13. Non-dimensional (*a*) volume flux and (*b*) specific momentum flux as a function of vertical position for plumes with intermediate and strong chemical reaction. Comparison between experimental measurements and theoretical predictions.

CO_2-laden seawater decreases the overall plume buoyancy, thereby changing the flow within and around a CO_2 plume. At various points in its ascent in a stratified ocean, heavy CO_2-enriched seawater laden with hydrate particles detrains away from the plume and subsides to a level of neutral buoyancy. This CO_2-enriched seawater is subsequently diluted and dispersed by ocean turbulence and currents, whilst some of the dense particles settle towards the ocean floor. Above a depth of approximately 500 m, any remaining CO_2 droplets vapourize and a two-phase bubble plume is formed.

In this section we use our model for a plume with heterogeneous chemical reaction to assess the relative influences of ocean stratification and of CO_2 dissolution on the dynamics of such CO_2 plumes. If we neglect the effects of the initial volume and momentum fluxes, we expect the behaviour of a CO_2 plume to be determined by the magnitude of N/G. The magnitude of G as a function of bubble/droplet diameter and depth of injection of CO_2 in the ocean can be estimated from (2.15). The actual bubble/droplet diameter at the source of the plume will in general depend on the design of the injection nozzle and on the injection rate of CO_2, as well as on the viscosity and density of the two phases, and the surface tension between them (Clift, Grace & Weber 1978). Further away from the source, the turbulence in the

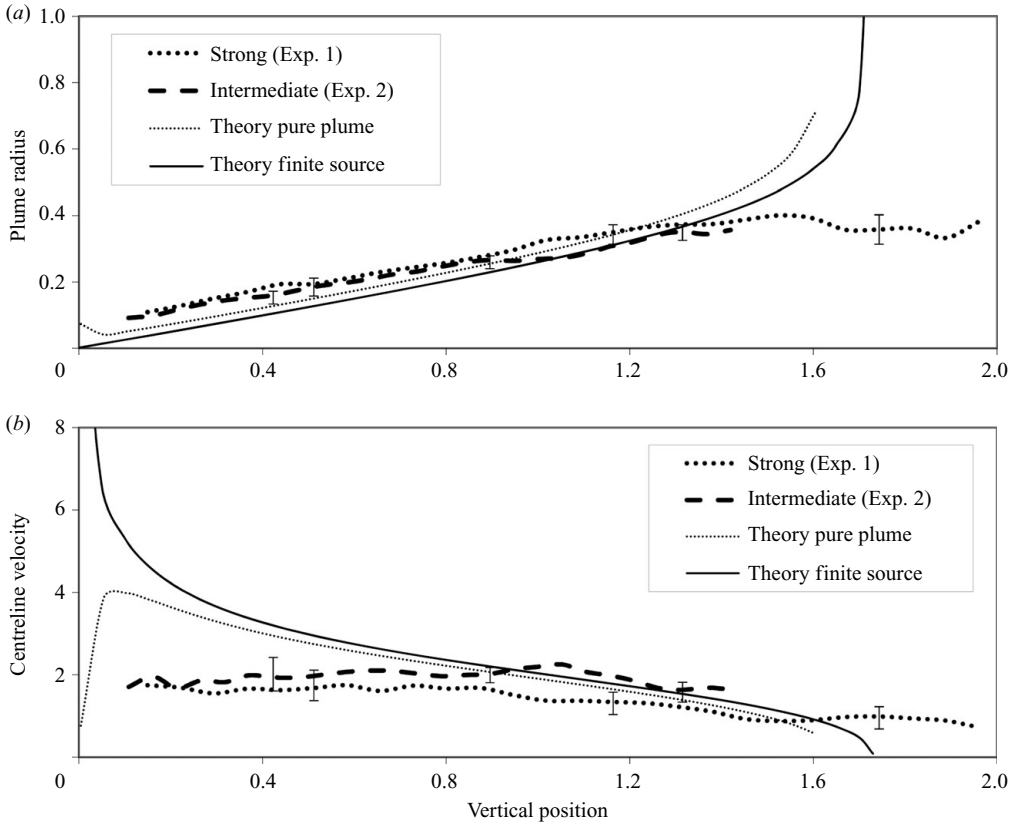

FIGURE 14. Non-dimensional (*a*) plume radius and (*b*) centreline velocity as a function of vertical position for plumes with intermediate and strong chemical reaction. Comparison between experimental measurements and theoretical predictions.

plume can contribute to bubble/droplet breakup. It is therefore difficult to predict theoretically the bubble/droplet size in a CO_2 plume. However, estimates for the droplet diameter, based on breakup due to Rayleigh–Taylor instability and shear stress in the plume, suggest an upper bound of 3 cm. We have therefore considered bubble/droplet diameters in the range of 0.5–2.5 cm.

The rate of dissolution of CO_2 from the droplet into the surrounding seawater, r, was estimated using the empirical work of Zhang (2005) and the experiments of Brewer *et al.* (2002), and is shown in figure 15 as a function of depth; here, r takes into account hydrate formation at depths larger than 490 m. The rate of dissolution is most influenced by pressure when CO_2 is in the gaseous phase (depths smaller than 492 m) and by temperature at depths where it is liquid; the effect of droplet diameter is small. Also shown in figure 15 are the densities of CO_2 and seawater as a function of depth. The variation of CO_2 density with temperature and pressure was calculated using Span and Wagner's equation of state (Span & Wagner 1996). The temperature and salinity as a function of depth were taken as those for the northeast Atlantic Ocean, as an example, and the seawater density was calculated using the UNESCO equation of state for seawater (Millero & Poisson 1981). Using the results above, the predicted magnitude of G as a function of bubble/droplet diameter, for various depths in the ocean, is presented in figure 16. The change in seawater density due to

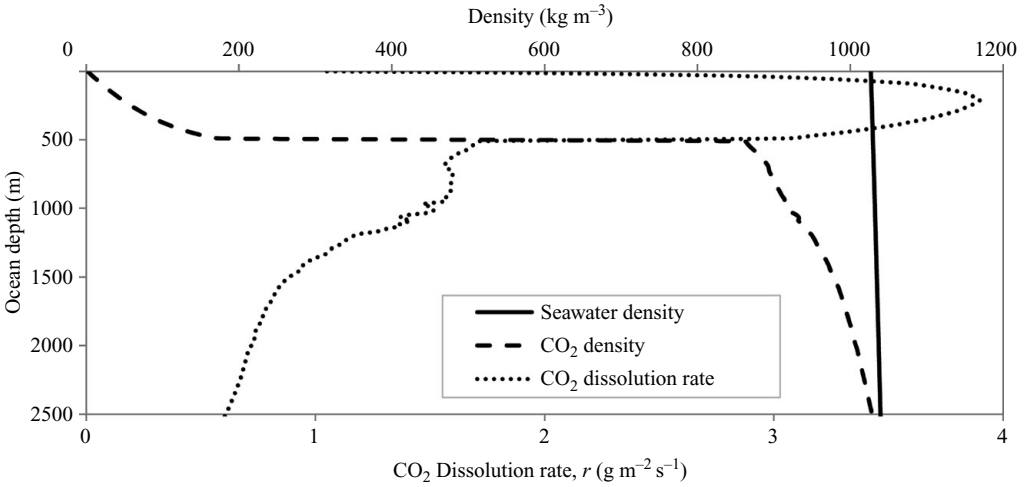

FIGURE 15. Seawater density, CO_2 density and dissolution rate of CO_2 in seawater, as a function of depth, for the temperature and salinity profiles in the northeast Atlantic.

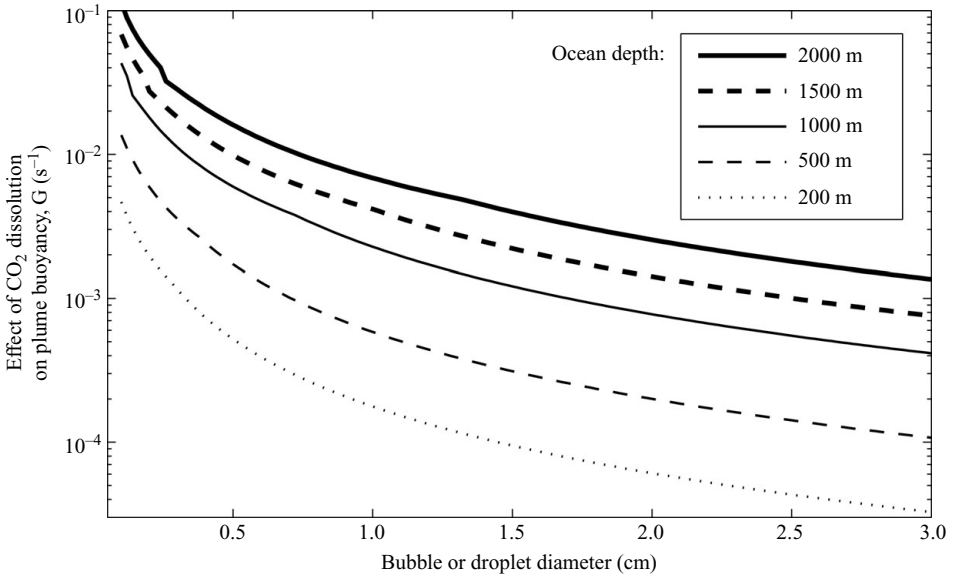

FIGURE 16. Effect of CO_2 dissolution on the buoyancy of the plume G as a function of CO_2-bubble/droplet diameter for ocean depths in the range 200–2000 m.

dissolved CO_2, required for the calculation of K_i in (2.6) and (2.15), was obtained from Ohsumi *et al.* (1992). The results for G indicate that the change of buoyancy in the plume, as a result of CO_2 dissolution and reaction with seawater, is larger for small bubbles/droplets and for a deep injection of CO_2. This trend is expected since G is inversely proportional to the droplet radius and to the density difference between CO_2 and seawater (cf. (2.15)); the latter decreases with depth, as seen in figure 15. We estimate further that for a plume of CO_2 droplets at depths between 1000 and 2000 m, $3k\nu_A/R \sim 10^{-4}\,\mathrm{s}^{-1}$ and $G \sim 10^{-3} - 10^{-2}\,\mathrm{s}^{-1}$; the criterion $|G| \gg 3k\nu_A/R$ (cf.

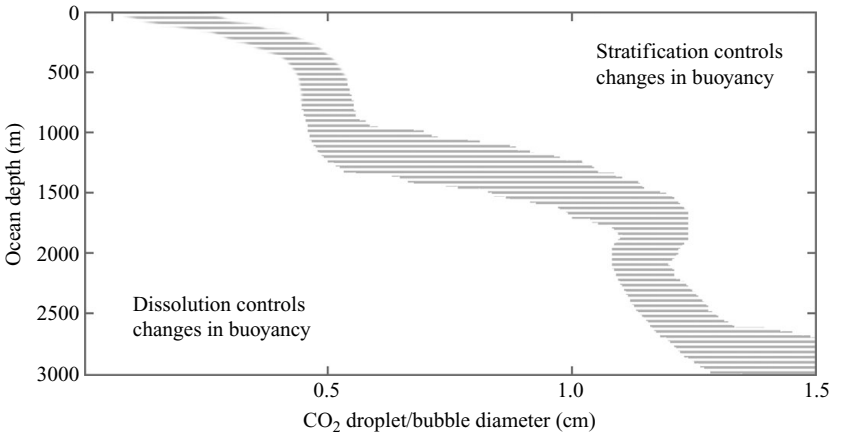

FIGURE 17. Comparison of the relative influences of seawater stratification and of dissolution of CO_2 on plume buoyancy. The dashed region corresponds to $N/G = 1 \pm 0.1$.

(2.16)) for negligible consumption of CO_2 is therefore satisfied and we may assume approximately constant droplet radius between detrainments. However, above 492 m depth, the CO_2 droplets vapourize and $3k\nu_A/R$ can become significantly larger than $|G|$. The theoretical predictions of our model are therefore applicable to a plume of CO_2 droplets but should be seen with more caution for a plume of CO_2 bubbles for which the rate of dissolution may become too large.

The relative influence of density stratification in the ocean and of dissolution of CO_2 on the plume's buoyancy is shown for various ocean depths and CO_2 droplet sizes in figure 17. In the dashed region, the relative influence of dissolution and stratification is approximately equivalent, that is, $N/G \sim 1$; for large droplets and a shallow release, the effects of stratification determine plume motion, but for small droplets and large release depths, the process of CO_2 dissolution controls the change of buoyancy in the plume.

We may also use the appropriate length scales for the plume motion in the reaction-dominant and stratification-dominant regimes, derived from (2.11), (2.12) and (2.17), to predict the typical ascent distances between detrainments of a plume of CO_2 droplets, for shallow- and deep-ocean conditions. For the reaction-dominant regime, the length scale is given by (2.19*c*), $L = (8\pi\alpha^2\gamma^{-1})^{-1/4}B_0^{1/4}|G|^{-3/4}$. When stratification in the environment has the dominant effect on changing the plume buoyancy, we can show that the appropriate length scale is $L_{ss} = (8\pi\alpha^2\gamma^{-1/2})^{-1/4}B_0^{1/4}N^{-3/4}$. For a release scenario of 13.3 kg s^{-1} of CO_2, which corresponds to one tenth of the output of a 500 MW coal or natural gas power plant, and a droplet diameter of 1 cm, we predict that detrainments will repeat over a length scale of 10–20 m for deep ocean releases in which dissolution and hydrate formation controls the plume flow. For shallow ocean releases, detrainments will occur less frequently at ascent distances separated by typically 50–100 m.

8. Conclusions

The fluid dynamics of a turbulent plume with heterogeneous reaction has been investigated. We developed a model for the case of a first-order irreversible reaction taking place at the surface of the dispersed, buoyant phase. This model complements the recent work of Conroy & Llewellyn Smith (2008) for a plume with second-order

homogeneous chemical reaction, for which the buoyancy change due to reaction is proportional to the product of the fluxes of the two reactants divided by the momentum flux. We show that for a heterogeneous reaction, with negligible consumption of reactant, the plume dynamics is different because the buoyancy change due to reaction is proportional to the ratio of the flow rate and momentum flux in the plume. In this case the behaviour of the plume is fully determined by the buoyancy frequency in the ambient, N, and the reaction frequency parameter G. In a uniform environment, a pure plume with a reaction that depletes buoyancy reaches a neutral buoyancy level given by $z_{B=0} = 1.31(8\pi\alpha^2\gamma^{-1})^{-1/4} B_0^{1/4} |G|^{-3/4}$. This relation is similar to that obtained by Morton *et al.* (1956) for an inert plume rising in a stratified environment, where N appears to the power $-3/4$ instead of G. In spite of this similarity, the effects of stratification and chemical reaction on a plume are rather different: the rate of change of buoyancy due to stratification increases with velocity in the plume, whilst the change in buoyancy due to reaction is larger when the plume moves slowly. Our theoretical predictions compare well with PIV measurements for a plume of calcium carbonate particles descending in an acidic solution. It was found that turbulent transport, owing to the presence of particles, was significant but within previously measured values for bubble plumes. In a stratified environment, the plume motion is bounded no matter how large the generation of buoyancy by reaction. The level of neutral buoyancy is in this case also proportional to $B_0^{1/4}|G|^{-3/4}$ but the coefficient of proportionality decreases with the ratio N/G.

We applied our model to the release of carbon dioxide in the ocean. It was shown that for a shallow injection and large CO_2 droplet sizes, the effects of stratification determine plume motion, but for small droplets and large release depths, the process of CO_2 dissolution controls the change of buoyancy in the plume. Such a plume would detrain the heavy CO_2-rich water more frequently at depth than near the surface of the ocean.

Funding from the Royal Society (RSRG 23838) and the Gates Cambridge Trust are gratefully acknowledged. The authors would like to thank Professor M. R. Mackley for providing the PIV equipment.

REFERENCES

Agrawal, A. & Prasad, A. K. 2004 Evolution of a turbulent jet subjected to volumetric heating. *J. Fluid Mech.* **511**, 95–123.

Asaeda, T & Imberger, J. 1993 Structure of bubble plumes in linearly stratified environments. *J. Fluid Mech.* **249**, 35–57.

Batchelor, G. K. 1954 Heat convection and buoyancy effects in fluids. *Q. J. R. Meteorol. Soc.* **80**, 339–358.

Bhat, G. S. & Narasimha, R. A. 1996 volumetrically heated jet: large-eddy structure and entrainment characteristics. *J. Fluid Mech.* **325**, 303–330.

Brewer, P., Peltzer, E., Friedrich, G. & Rehder, G. 2002 Experimental determination of the fate of rising CO_2 droplets in seawater. *G. Environ. Sci. Technol.* **36**, 5441–5446.

Carazzo, G., Kaminski, E. & Tait, S. 2006 The route to self-similarity in turbulent jets and plumes. *J. Fluid Mech.* **547**, 137–148.

Chen, M. H. & Cardoso, S. S. S. 2000 The mixing of liquids by a plume of low Reynolds number bubbles. *Chem. Engng Sci.* **55**, 2585–2594.

Chen, J. C. & Rodi, W. 1980 *Turbulent Buoyant Jets – A Review of Experimental Data.* Pergamon Press.

Clarke, J. F. & Mcchesney, M. 1964 *The Dynamics of Real Gases.* Butterworth.

Clift, R., Grace, J. R. & Weber, M. E. 1978 *Bubbles, Drops, and Particles.* Academic Press.

Conroy, D. T. & Llewellyn Smith, S. G. 2008 Endothermic and exothermic chemically reacting plumes. *J. Fluid Mech.* **612**, 291–310.

Diez, F. J. & Dahm, W. J. A. 2007 Effects of heat release on turbulent shear flows. Part 3. Buoyancy effects due to heat release in jets and plumes. *J. Fluid Mech.* **575**, 221–255.

Fairlie, R. & Griffiths, J. F. 2001 A numerical study of spatial structure during oscillatory combustion in closed vessels in microgravity. *Faraday Discuss.* **120**, 147–164.

Hunt, G. R. & Kaye, N. B. 2005 Lazy plumes. *J. Fluid Mech.* **533**, 329–338.

Ishimine, Y. 2007 A simple integral model of buoyancy-generating plumes and its application to volcanic eruption columns. *J. Geophys. Res.* **112**, B03210.

Kaminski, E., Tait, S. & Carrazo, G. 2005 Turbulent entrainment in jets with arbitrary buoyancy. *J. Fluid Mech.* **526**, 361–76.

Linden, P. F. 2000 Convection in the environment. In *Perspectives in Fluid Dynamics* (ed. G. K. Batchelor, H. K. Moffat & M. G. Worster), pp. 289–345. Cambridge University Press.

Liu, T. Y., Campbell, A. N., Cardoso, S. S. S. & Hayhurst, A. N. 2008. Effects of natural convection on thermal explosion in a closed vessel. *Phys. Chem. Chem. Phys.* **10**, 5521–5530.

McDougall, T. J. 1978 Bubble plumes in stratified environments. *J. Fluid Mech.* **85**, 655–672.

Metz, B., Davidson, O., de Coninck, H., Loos, M. & Meyer, L. (Ed.) 2005 *Carbon Dioxide Capture and Storage*. Cambridge University Press.

Milgram, J. H. 1983 Mean flow in round bubble plumes. *J. Fluid Mech.* **133**, 345–376.

Millero, F. J. & Poisson, A. 1981 International one-atmosphere equation of state of seawater. *Deep-Sea Res.* **28**, 625–629.

Morton, B. R., Taylor, G. I. & Turner, J. S. 1956 Turbulent gravitational convection from maintained and instantaneous sources. *Proc. R. Soc.* **234**, 1–23.

Ohsumi, T., Nakashiki, N., Shitashima, K. & Hirama, K. 1992 Density change of water due to dissolution of carbon dioxide and near-field behaviour of CO_2 from a source on the deep-sea floor. *Energy Convers. Manage.* **33**, 685–690.

Papanicolaou, P. N. & List, E. J. 1988 Investigations of round vertical turbulent buoyant jets. *J. Fluid Mech.* **195**, 341–91.

Priestley, C. H. B. & Ball, F. K. 1955 Continuous convection from isolated source of heat. *Q. J. R. Mech. Soc.* **81**, 144–157.

Sandler, S. I. 1999 *Chemical and Engineering Thermodynamics*. Wiley.

Scase, M. M., Caulfield, C. P. & Dalziel, S. B. 2006*a* Boussinesq plumes with decreasing source strengths in stratified environments. *J. Fluid Mech.* **563**, 463–472.

Scase, M. M., Caulfield, C. P. & Dalziel, S. B. 2008 Temporal variation of non-ideal plumes with sudden reductions in buoyancy flux. *J. Fluid Mech.* **605**, 181–199.

Scase, M. M., Caulfield, C. P., Dalziel, S. B. & Hunt, J. C. R. 2006*b* Time-dependent plumes and jets with decreasing source strengths. *J. Fluid Mech.* **563**, 443–461.

Socolofsky, S. A. & Adams, E. E. 2005 Role of slip velocity in the behaviour of stratified multiphase plumes. *J. Hydr. Engng* **131** (4), 273–282.

Span, R. & Wagner, W. 1996 A new equation of state for carbon dioxide covering the fluid region from triple-point temperature to 1100 K at pressures up to 800 MPa. *J. Phys. Chem. Ref. Data* **25** (6), 1509–1596.

Turner, J. S. 1966 Jets and plumes with negative or reversing buoyancy. *J. Fluid Mech.* **26**, 779–792.

Turner, J. S. 1979 *Buoyancy Effects in Fluids*. Cambridge University Press.

Wang, H. & Law, A. W.-K. 2002 Second-order integral model for a round turbulent buoyant jet. *J. Fluid Mech.* **459**, 397–428.

Woods, A. W. & Caulfield, C. P. 1992 A laboratory study of explosive volcanic eruptions. *J. Geophys. Res.* **97**, 6699–6712.

Zarrebini, M. & Cardoso, S. S. S. 2000 Patterns of sedimentation from surface currents generated by turbulent plumes. *AIChE J.* **46** (10), 1947–1956.

Zhang, Y. 2005 Fate of rising CO_2 droplets in seawater. *Environ. Sci. Technol.* **39**, 7719–7724.